Nuclear phosphatidylinositol 4,5-bisphosphate islets contribute to efficient RNA polymerase II-dependent transcription

Margarita Sobol[1], Alžběta Krausová[1], Sukriye Yildirim[1], Ilona Kalasová[1], Veronika Fáberová[1], Vladimír Vrkoslav[2], Vlada Philimonenko[1,3], Pavel Marášek[1], Lukáš Pastorek[1,3], Martin Čapek[4], Zuzana Lubovská[3], Lívia Uličná[1], Takuma Tsuji[5], Miroslav Lísa[6], Josef Cvačka[2], Toyoshi Fujimoto[5], Pavel Hozak[1,7,8]

[1]Institute of Molecular Genetics, CAS, v.v.i., Department of Biology of the Cell Nucleus, Vídeňská 1083, 142 20, Prague 4, Czech Republic

[2]Institute of Organic Chemistry and Biochemistry, CAS, v.v.i., Research Service Group of Mass Spectrometry, Flemingovo náměstí 2, 166 10, Prague 6, Czech Republic

[3]Institute of Molecular Genetics, CAS, v.v.i., Electron Microscopy Core Facility, Vídeňská 1083, 142 20, Prague 4, Czech Republic

[4]Institute of Molecular Genetics, CAS, v.v.i., Light Microscopy Core Facility, Vídeňská 1083, 142 20, Prague 4, Czech Republic

[5]Nagoya University Graduate School of Medicine, Department of Molecular Cell Biology, 65 Tsurumai-cho, Showa-ku, Nagoya 466-8550, Japan

[6]University of Pardubice, Faculty of Chemical Technology, Department of Analytical Chemistry, Studentská 573, 532 10, Pardubice, Czech Republic

[7]Institute of Molecular Genetics, CAS, v.v.i., Division BIOCEV, Laboratory of Epigenetics of the Cell Nucleus, Průmyslová 595, 252 50, Vestec, Czech Republic

[8]Institute of Molecular Genetics, CAS, v.v.i., Microscopy Centre, Vídeňská 1083, 142 20, Prague 4, Czech Republic

Corresponding author: Pavel Hozak, hozak@img.cas.cz

Tel: +420 241 062 219

Fax: +420 241 062 289

JCS Advance Online Article. Posted on 5 March 2018

Abstract

This paper describes a novel type of nuclear structures – nuclear lipid islets (NLIs). They are of 40–100 nm with a lipidic interior, and PtdIns(4,5)P_2 molecules comprise a significant part of their surface. Most of NLIs have RNA at the periphery. Consistently with that, RNA is required for their integrity. NLI periphery is associated with Pol II transcription machinery, including the Pol II largest subunit, transcription factors, and NM1. The PtdIns(4,5)P_2–NM1 interaction is significant for Pol II transcription, since NM1 knock-down reduces the Pol II transcription level, and the overexpression of wild-type NM1 (but not NM1 mutated in the PtdIns(4,5)P_2-binding site) rescues the transcription. Importantly, Pol II transcription is dependent on NLI integrity, because an enzymatic reduction of the PtdIns(4,5)P_2 level results in a decrease of the Pol II transcription level. Furthermore, about a half of nascent transcripts localise to NLIs, and transcriptionally active transgene loci preferentially colocalise with NLIs. We hypothesize that NLIs serve as a structural platform, which facilitates the formation of Pol II transcription factories, thus participating in the formation of nuclear architecture competent for transcription.

Keywords: nucleus, PtdIns(4,5)P_2, DNA transcription, chromatin, RNA polymerase II, phosphoinositides

Summary Statement

This is the first study to describe a novel nuclear structure - nuclear lipid islets (NLIs). NLIs might serve as a structural platform, which facilitates the formation of Pol II transcription factories, thus participating in the formation of nuclear architecture competent for transcription.

Introduction

Phosphoinositides are amphipathic lipids containing a hydrophilic inositol head group and hydrophobic fatty acid tails. Phosphatidylinositol 4,5-bisphosphate (PtdIns(4,5)P_2) is a phosphoinositide phosphorylated at the 4C and 5C hydroxyl groups of the inositol ring (Balla, 2013; Tanaka et al., 2003). PtdIns(4,5)P_2 predominantly localises to the plasma membrane, where it participates in signalling (Balla, 2013). In addition, PtdIns(4,5)P_2 is present also in the cell nucleus together with the enzymes and substrates involved in its metabolism. In striking contrast to the cytoplasm, nuclear PtdIns(4,5)P_2 is exclusively localised in the nuclear interior and is absent from the nuclear membrane (Cocco et al., 1987; Payrastre et al., 1992; Vann et al., 1997). Under extraction with high detergent concentrations, nearly half of the PtdIns(4,5)P_2 amount is retained in the nucleus. This implies that PtdIns(4,5)P_2 might be bound in larger intranuclear complexes (Gonzales and Anderson, 2006; Vann et al., 1997). Indeed, it has been shown that PtdIns(4,5)P_2 promotes the interaction of chromatin-remodelling SWI/SNF-like BAF complex with chromatin, which leads to T-lymphocyte activation (Zhao et al., 1998). To some extent, this effect is exerted through the binding of PtdIns(4,5)P_2 to the BRG1 subunit of the BAF complex and changing the conformation of β-actin thus enhancing the binding of the BAF complex to actin filaments (Rando et al., 2002). There are also notions that PtdIns(4,5)P_2 is involved in cell differentiation (Cocco et al., 1987), cell growth (Divecha et al., 1991), and cell division (Geeraerts et al., 2013). Recently, we showed that PtdIns(4,5)P_2 interacts with the upstream binding factor (UBF) of RNA polymerase I (Pol I) and fibrillarin and triggers their conformational changes thus affecting their binding to ribosomal RNA (rRNA) genes and rRNA, respectively (Yildirim et al., 2013). Remarkably, PtdIns(4,5)P_2 is associated with Pol I subunits RPA116 and PAF53 as well as with UBF independent of Pol I activity. In mitotic chromosomes, PtdIns(4,5)P_2 is present as a lipidic component of the nucleolar organising region (NOR) complex (Sobol et al., 2013). PtdIns(4,5)P_2 might be expected to be similarly involved in the organisation of RNA polymerase II (Pol II) transcription complexes. It is noteworthy that a number of papers describe the diverse effects of PtdIns(4,5)P_2 on Pol II transcription. The predominant association of PtdIns(4,5)P_2 with hyperphosphorylated Pol II was shown (Osborne et al., 2001). PtdIns(4,5)P_2 regulates the processivity of poly(A) polymerase Star-PAP thus controlling mRNA 3' processing and influencing mRNA expression (Mellman et al., 2008). PtdIns(4,5)P_2 binding to histone H1 was revealed to result in the dissociation of H1 from DNA thus promoting transcription in the *Drosophila* embryo transcription system (Yu et al., 1998). On the contrary, PtdIns(4,5)P_2 is engaged in the recruitment of histone deacetylase 1 to the transcriptional co-factor BASP1 at the promoter of WT1 target genes, thus eliciting transcriptional repression (Toska et al., 2012). These data suggest that the nuclear PtdIns(4,5)P_2 may exert various effects depending on its interactions with particular proteins or complexes. However, the precise mechanisms of PtdIns(4,5)P_2 participation in Pol II transcription remain unclear.

In order to associate with the hydrophilic part of PtdIns(4,5)P_2, many proteins contain specific motifs enriched in basic amino acids, such as the PH (pleckstrin homology) domain or the PDZ (postsynaptic density protein, disc-large, zona occludens) domain (Geeraerts et al., 2013; Mortier et al., 2005; Watt et al., 2002). Other proteins are able to interact with the hydrophilic or hydrophobic parts of PtdIns(4,5)P_2 through as-yet-unknown moieties (Ferguson et al., 1995; Gonzales and Anderson, 2006; Harlan et al., 1994; Irvine, 2006; Lemmon et al., 1995; Mortier et al., 2005; Sugi et al., 2008; Wang et al., 2001; Zimmermann et al., 2002). Therefore, we searched for nuclear PtdIns(4,5)P_2-interacting proteins containing known PtdIns(4,5)P_2-binding motifs. One of such possible candidates is nuclear myosin 1 (NM1), which possesses a PH domain in the C-terminus and binds PtdIns(4,5)P_2 in the cytoplasm (Hokanson et al., 2006; Hokanson and Ostap, 2006). Previously, it has been shown that NM1 facilitates chromatin remodelling (Cavellan et al., 2006; Percipalle et al., 2006). The role of NM1 in rRNA biogenesis was well described (Philimonenko et al., 2004). Overexpression of a NM1 mutant lacking the C-terminal domain reduces the Pol I level at the rDNA promoter and the transcribed region, suggesting a role for the PtdIns(4,5)P_2-binding motif in transcription (Ye et al., 2008). The C-terminus of NM1 is also responsible for binding to rDNA and histone acetyl transferase PCAF as revealed using a NM1 C-terminal deletion mutant (Sarshad et al., 2013). However, in contrast to Pol I, the involvement of NM1 in Pol II transcription has been described only vaguely (Almuzzaini et al., 2015; Hofmann et al., 2006; Venit et al., 2013).

Here we studied the role of nuclear PtdIns(4,5)P_2 and NM1 in the organisation of Pol II transcription complexes. We show that nuclear PtdIns(4,5)P_2 associates with Pol II, transcription factors, nascent transcripts, and NM1 at the periphery of specialised nuclear structures – nuclear lipid islets (NLIs). The integrity of NLIs as well as the interaction of PtdIns(4,5)P_2 with NM1 are necessary for Pol II transcription. We demonstrate that PtdIns(4,5)P_2 is the major component of NLI periphery, while RNA, ceramide, and cholesterol constitute a minor part. We suggest that NLIs serve as a structural platform which facilitates the assembly of Pol II transcription-competent nuclear architecture.

Results

Nascent RNA and proteins involved in Pol II transcription colocalise with nucleoplasmic phosphatidylinositol 4,5-bisphosphate islets

Previously published data showed that PtdIns(4,5)P_2 is pulled down by Pol II (Osborne et al., 2001) and binds to Pol I transcription machinery (Sobol et al., 2013; Ulicna et al., 2018; Yildirim et al., 2013). These findings prompted us to study the particular transcription-related proteins associated with nucleoplasmic PtdIns(4,5)P_2. Using super-resolution microscopy, we analysed the colocalisation between PtdIns(4,5)P_2, the components of Pol II transcription machinery, and BrU-labelled nascent RNA (BrRNA). We found that the nucleoplasmic PtdIns(4,5)P_2 appears in small foci and colocalises with nascent BrRNA transcripts, the C-terminal domain (CTD) of the Pol II largest subunit, and the TATA-box binding protein (TBP) of the Pol II transcription factor TFIID (Fig. 1A,B). The extent of the colocalisation between PtdIns(4,5)P_2, nascent BrRNA, Pol II, and TFIID was documented by the high values of Manders' (MCC) and Pearson's (PCC) colocalisation coefficients (Fig. 1E,F). The relevance and usage of these coefficients are described in detail elsewhere (Bolte and Cordelieres, 2006; Dunn et al., 2011). In contrast to the specific colocalisation between nucleoplasmic PtdIns(4,5)P_2 foci and the components of the Pol II transcription complex, the non-interacting proteins, Son and Aurora B kinase, showed no colocalisation with these PtdIns(4,5)P_2 foci (Fig. 1C,D), which was documented by the low values of MCC and PCC (Fig. 1E,F; $p \leq 0.001$). We additionally verified our results by showing the high level of colocalisation between PtdIns(4,5)P_2 and Son in nuclear speckles (Fig. 1C,E,F). The nuclear speckle localisation of PtdIns(4,5)P_2 had been proved earlier (Osborne et al., 2001). Son was chosen as a marker of nuclear speckles (Lamond and Spector, 2003) based on its characteristics as a crucial nuclear speckle protein which serves as a scaffolding component and is essential for nuclear speckle integrity (Saitoh et al., 2004; Sharma et al., 2010). We confirmed and extended our findings by the specific association of PtdIns(4,5)P_2 with Pol II CTD (including its phosphorylated form at serine 5 – Pol II S5), Pol II transcription factor p62 (core subunit of TFIIH; TFIIH p62), the large subunit of TFIIE (TFIIEα), and TFIID TBP using immunoprecipitation with anti-PtdIns(4,5)P_2 antibody from the HeLa nuclear extract (Fig. 1G).

Another protein involved in Pol II transcription activation through the recruitment of chromatin-remodelling proteins and histone modification enzymes is NM1 (Almuzzaini et al., 2015; Hofmann et al., 2006). Transmission electron microscopy (TEM) showed more accurately that these PtdIns(4,5)P_2 foci are structures of 40–100 nm in size, and revealed the presence of NM1 at the periphery of these structures (Fig. 1H). We showed that the colocalisation between PtdIns(4,5)P_2 molecules and NM1 is significant at the distances of 25–75 nm ($p \leq 0.01$). In support of this, we found the specific association of PtdIns(4,5)P_2 with NM1 in the immunoprecipitation experiment as well (Fig. 1G).

In conclusion, nucleoplasmic PtdIns(4,5)P_2 decorates 40–100 nm structures, to which we refer as nuclear lipid islets (NLIs). They are associated with Pol II transcription machinery and might participate in transcription as suggested by the presence of nascent RNA.

The morphology, composition and distribution of NLIs

As this is the first definition of NLIs and we show that they may be involved in such functionally crucial process as DNA transcription, we analysed them in detail. First, we thoroughly mapped nuclear PtdIns(4,5)P_2 localisation by anti-PtdIns(4,5)P_2 antibody. Using super-resolution structured illumination microscopy (SIM), we acquired z-stacks, reconstructed the nuclei in three-dimensional space and analysed the distribution of PtdIns(4,5)P_2 labelling in the nuclear volume by the procedure described in the Materials and methods section (Fig. 2A). We used Son as a nuclear speckle-specific marker as well as histone H1 and DAPI as markers of the nucleoplasm. We revealed that ~68% of the total nuclear PtdIns(4,5)P_2 localises to nuclear speckles, while nucleolar PtdIns(4,5)P_2 constitutes ~4%. The remaining ~28% was located throughout the nucleoplasm. To visualise the nucleoplasmic pool of PtdIns(4,5)P_2 more accurately, we inspected it using the labelling with anti-PtdIns(4,5)P_2 antibody and TEM (Fig. 2B). We showed that nucleoplasmic PtdIns(4,5)P_2 is located at the periphery of NLIs, which can be clearly distinguished from the nuclear speckles by size (40–100 nm), unstructured interior, and their shape. NLIs have no discernible membrane (Fig. 2B). NLIs occupy 10.6±4.0 μm^3 per nucleus, which corresponds to 1.9±0.2% of the total nuclear volume. In agreement with previous studies, PtdIns(4,5)P_2 was absent from the nuclear envelope (Osborne et al., 2001; Thomas et al., 1999; Watt et al., 2002).

To uncover the composition of NLIs, we mapped the presence of nitrogen and phosphorus, which are the enriched elements in proteins and nucleic acids, respectively (Aronova and Leapman, 2012). We used electron energy loss spectroscopy (EELS) on ultrathin sections of U2OS cells immunolabelled with anti-PtdIns(4,5)P_2 antibody for NLI identification (Fig. 2C). We ascertained that NLIs are enclosed by phosphorus- and nitrogen-rich structures, whereas the inner space of NLIs lacks them both (Fig. 2D-F). On the contrary, the interior of NLIs is mainly composed of carbon-rich compounds (Fig. 2G). To study the lipidic component of NLIs in more detail, we used hydrophilic interaction liquid chromatography – ultrahigh-performance liquid chromatography/electrospray ionisation – mass spectrometry (HILIC-UHPLC/ESI-MS) modified from Holcapek et al. (2015) and immunoprecipitation with anti-PtdIns(4,5)P_2 antibody from the HeLa nuclear extract. We showed that the major lipidic constituents specifically associated with PtdIns(4,5)P_2 are phosphatidylcholines, phosphatidylethanolamines, triacylglycerols, and sphingomyelins ($p \leq 0.001$, $p \leq 0.001$, $p \leq 0.05$, and $p \leq 0.05$, respectively; Fig. 2H). These data together indicate that nucleic acids and proteins surround NLIs, which is in agreement with the results shown in Figs. 1, 4, 5, and 6, while lipids form the body of NLIs. Moreover, TEM in combination with immunogold labelling revealed nucleoplasmic

cholesterol and ceramide, decorating the periphery of NLIs (Fig. 2I,L). The colocalisation between PtdIns(4,5)P_2 molecules and both cholesterol and ceramide was significant at the distance of 25–75 nm ($p \leq 0.01$; Fig. 2J,M). Interestingly, the analysis of the relative colocalisation of nucleoplasmic cholesterol and ceramide with PtdIns(4,5)P_2 molecules on resin sections demonstrated that ~70% of either cholesterol or ceramide is colocalised with NLIs ($p \leq 0.01$ and $p \leq 0.001$, respectively). On the other hand, only about one-third of NLIs contains cholesterol, and one-fourth of NLIs contains ceramide (Fig. 2K,N).

These immunolabelling TEM experiments were performed using resin-embedded samples of either chemically fixed or high-pressure frozen cells. To ensure that NLIs, which are the focus of our study, are not artefacts of the sample preparation but indeed native structures, we performed quick-freezing/freeze-fracture replica labelling (QF-FRL). This is the only ultrastructural method known so far to maintain the native localisation of lipid molecules due to their fixation at the metallic layer of replica. We used HeLa cells and labelled the replicas with either anti-PtdIns(4,5)P_2 antibody or the PH domain of 1-phosphatidylinositol-4,5-bisphosphate phosphodiesterase delta-1 (PLC PH domain) to detect PtdIns(4,5)P_2. Also here, TEM clearly revealed PtdIns(4,5)P_2 and ceramide at the periphery of NLIs (Fig. 2O,P), which further confirmed our observations using different procedures described above (Fig. 2B,C,L). Therefore, we conclude that NLIs are native nuclear structures.

We summarise that ~28% of nuclear PtdIns(4,5)P_2 is located throughout the nucleoplasm, forming the outer layer of NLIs. NLIs are structures of 40–100 nm in size and occupy 10.6±4.0 μm^3 per nucleus, which is 1.9±0.2% of the total nuclear volume. NLIs have the lipidic interior surrounded by proteins and nucleic acids.

NM1 associates with NLIs and is anchored in nucleoplasm by PtdIns(4,5)P_2

As we detected NM1 at the periphery of NLIs as well as in specific association with PtdIns(4,5)P_2 (Fig. 1G,H), and based on the fact that NM1 contains a PH domain, which mediates its interaction with cytoplasmic PtdIns(4,5)P_2 (Hokanson et al., 2006; Hokanson and Ostap, 2006), we studied the details of NM1-PtdIns(4,5)P_2 interactions in the nucleus. First, we pulled down NM1 from the HeLa nuclear extract (Fig. 3A) using PtdIns(4,5)P_2-coupled agarose beads (Fig. 3B). To see whether this interaction is direct, we prepared a recombinant wild-type NM1 as well as NM1 mutated in the PH domain – NM1(K908A), and verified their PtdIns(4,5)P_2-binding ability using PtdIns(4,5)P_2 spotted on a nitrocellulose membrane. Unlike the wild-type NM1, NM1(K908A) showed no reaction with PtdIns(4,5)P_2 (Fig. 3C). Therefore, the mutation in the PH domain prevents the binding of NM1 to PtdIns(4,5)P_2 and this interaction is direct. To ensure the equal loading of both NM1 and NM1(K908A) used for this experiment, we monitored their amount by SDS-PAGE (Fig. 3D).

To demonstrate that NM1 is anchored to NLIs, we performed a flotation of extracted HeLa nuclei on a sucrose density gradient in the presence of a weak non-ionic detergent Brij 98. During high-

speed ultracentrifugation, the density gradient spontaneously forms and the constituents of the HeLa nuclear extract are distributed within the sucrose gradient according to their lipid and protein content. In such a way, lipid-rich complexes float to the top, where the sucrose concentration is the lowest; therefore, they are called the 'light fraction'. At the same time, detergent-soluble complexes and components extracted by Brij 98 remain within the densest sucrose fraction, located at the bottom; therefore, they are called the 'heavy fraction'. By western blotting and dot blotting, we found that both NM1 and PtdIns(4,5)P_2 are present in the light fraction (number 1, Fig. 3E), which contains detergent-insoluble complexes, composed of lipids and proteins. NM1 and PtdIns(4,5)P_2 were also present in the heavy fraction (number 10, Fig. 3E), which corresponds to complexes solubilised by detergent. Additionally, using western blotting, we tested the fractions for the presence of Pol II and Pol I. Pol II CTD and RPA194 (the largest subunit of Pol I) were predominantly enriched in the detergent-soluble heavy fraction (number 10, Fig. 3E), suggesting that they are not the essential components of lipid complexes.

We conclude that NM1 is anchored in the nucleoplasm by PtdIns(4,5)P_2-containing structures. Taking into account also the electron microscopy results of the colocalisation between PtdIns(4,5)P_2 and NM1 (Fig. 1H), we can conclude that the majority of these structures are NLIs and NM1 is anchored at their surface.

PtdIns(4,5)P_2–NM1 interaction and integrity of NLIs are important for Pol II-dependent transcription

NM1 is known to associate with Pol II (Hofmann et al., 2006; Venit et al., 2013), however the details of this interaction are not clear. When we used the mutated NM1(K908A), we observed a loss of association with Pol II, as tested by immunoprecipitation (Fig. 4A). Therefore, we also studied the effect of this NM1 mutation on Pol II transcription. For this experiment, cell lines stably expressing either shRNA only or in combination with shRNA-resistant NM1-flag/shRNA-resistant NM1(K908A)-flag were prepared by lentiviral transduction. We pulse-labelled nascent transcripts with fluorouridine (FU) *in vivo* in these cell lines for 30 min and quantified the signal intensity by indirect immunofluorescence microscopy. Our results revealed that the depletion of NM1 by shRNA-mediated knock-down (Fig. 4B) significantly reduced Pol II transcription by ~33% (Fig. 4C). The overexpression of shRNA-resistant NM1 rescued Pol II transcription close to its original level. In contrast, the overexpression of shRNA-resistant NM1(K908A) did not rescue Pol II transcription, which remained at the knocked-down level. Thus we suggest that NM1 requires PtdIns(4,5)P_2 in order to associate with Pol II and to participate in the transcription.

Since NM1 and the components of Pol II transcription machinery are associated with NLIs, we investigated whether the integrity of NLIs is important for DNA transcription at their periphery. To disintegrate NLIs, we treated the permeabilised U2OS cells with PLC (Fig. S1). Upon PtdIns(4,5)P_2 hydrolysis, we quantified the level of transcription using the indirect immunofluorescence microscopy of FU-labelled nascent RNA (FRNA). For this and all following colocalisation analyses, we considered only nucleoplasmic regions devoid of nucleoli and nuclear speckles, which we referred to as the 'NLI area'. In immunofluorescent experiments, the area of nuclear speckles was excluded based on the labelling by a nuclear speckle-specific marker, Son. We showed that reducing the PtdIns(4,5)P_2 level by hydrolysis down to ~40% resulted in a decrease of the Pol II transcription level by ~55% in the NLI area (Fig. 4D). The mutated PLC(R40A) with abolished binding to PtdIns(4,5)P_2, heat-inactivated PLC or irrelevant protein BSA did not substantially affect the level of transcription by Pol II.

Altogether, our results indicate that Pol II transcription is dependent on the presence of intact NLIs. In support, TEM has clearly demonstrated that nascent BrRNA transcripts localise at the periphery of NLIs (Fig. 4E). The colocalisation between PtdIns(4,5)P_2 molecules and nascent BrRNA transcripts was significant for distances 25–75 nm; $p \leq 0.01$ (Fig. 4F). Furthermore, the analysis of the relative colocalisation of BrRNA and PtdIns(4,5)P_2 molecules on resin sections showed that almost half of nascent RNA transcripts are colocalised with NLIs ($p \leq 0.001$; Fig. 4G). On the other hand, only a minor part of NLIs (~9%) are colocalised with BrRNA. Interestingly, the inhibition of Pol II transcription did not significantly alter either the pattern or the quantity of NLIs per μm^2 as compared to the control (Fig. 4H,I).

In conclusion, Pol II transcription is dependent on the integrity of NLIs, and a substantial portion of transcription activity occurs at their periphery, where PtdIns(4,5)P_2 mediates the interaction of NM1 with the Pol II transcription complex. NLIs are numerous in the nucleoplasm, they appear structurally independent of ongoing transcription, and only a part of them is associated with active transcription. We suggest that NLIs serve as a structural platform which facilitates the formation of the various complexes involved in Pol II transcription at their periphery.

NLIs are chromatin-independent but RNA-associated structures

Above, we demonstrated the relationship between NLIs and Pol II transcription. To reveal the possible preferences in the association of NLIs with chromatin on their surface, we performed a colocalisation of NLIs with histones H3K4me2 and H3K9me2, the hallmarks of active chromatin and heterochromatin, respectively. Using immunolabelling followed by SIM, we showed that NLIs partially overlap with both histone marks with no preference for either type of chromatin (Fig. 5A,B).

To test whether NLIs are indeed chromatin-independent structures, we studied the pattern of NLIs upon DNase treatment. NLIs appeared resistant to DNase, and they were arranged in a similar pattern in both control and DNase-treated cells (Fig. 5C,D). Since we demonstrated that NLIs colocalise with nascent RNA transcripts (Figs 1A,B,E,F; 4E-I), we also studied the effect of RNase on the arrangement of NLIs. Surprisingly, the treatment of cells with RNase caused a complete disappearance of NLI labelling (Fig. 5E). These results encouraged us to assess the overall association of RNA molecules with NLIs by TEM. We simultaneously labelled PtdIns(4,5)P_2 and total RNA with anti-PtdIns(4,5)P_2 antibody and RNase conjugated to gold nanoparticles – the RNase-gold complex (Fig. S2A,B). TEM revealed that RNA molecules are located on the surface of NLIs (Fig. 5F). For TEM colocalisation analyses, the 'NLIs area' was distinguished from nuclear speckles and nucleoli based on the ultrastructure and the pattern of PtdIns(4,5)P_2 labelling. The colocalisation of RNA and PtdIns(4,5)P_2 molecules was significant ($p \leq 0.01$) at the distance of 25–75 nm. Moreover, the analysis of their relative colocalisation showed that ~73% of NLIs is colocalised with RNA molecules, while only ~22% of RNA molecules is colocalised with NLIs ($p \leq 0.001$; Fig. 5G).

In summary, DNA is not required for the integrity of NLIs, but RNA is an essential component for their integrity. RNA, however, does not form the core of NLIs but associates with their surface.

Transcriptionally active genes are preferentially positioned on the surface of NLIs

Because NLIs are structurally independent of chromatin and ongoing transcription, while RNA is their crucial component, we asked whether the functional changes in the transcriptional status of genes affect their position relative to NLIs. We used U2OS cells stably expressing a plasmid containing a *lac* operator (LacO), tetracycline response elements, a CMV minimal promoter, and CFP with peroxisomal targeting signal-1 [Ser-Lys-Leu (SKL)] (Janicki et al., 2004). We co-transfected the cells with the tetracycline-controlled transactivator and the EYFP-lac repressor, and induced the transcription by the addition of doxycycline (dox) to the medium. Then we pulse-labelled nascent transcripts with FU *in vivo*, fixed the cells and immunolabelled them with antibodies against PtdIns(4,5)P_2 and FU. The induction of transcription was controlled by the appearance of CFP-SKL in the cytoplasmic peroxisomes (Fig. S3A,B) and by the characteristic changes in the arrangement of transgene foci (Fig. S3C,D). Stimulated emission depletion super-resolution microscopy (STED) revealed that in the absence of dox, the transcriptionally silent transgene locus does not colocalise with either NLIs or the nascent transcripts (Fig. 6A). Upon transcription induction, the decondensed locus clearly colocalised with NLIs and nascent transcripts (Fig. 6B). By means of image processing and statistics, we then analysed in detail the colocalisation between the transgene locus, nascent transcripts, and each NLI. Using PCC, we showed that the level of colocalisation for all three pairs (Fig. 6C,D): transgene foci (LacO) and NLIs, nascent transcripts (FRNA) and NLIs, transgene foci and nascent transcripts - is statistically significantly higher upon transcription induction ($p \leq 0.01$, $p \leq 0.001$, and $p \leq 0.001$, respectively; Fig. 6E). We confirmed these results using MCC and showed that the induction of transcription evoked an increased extent of colocalisation of all three tested patterns: 1) between transgene foci (LacO) and NLIs ($p \leq 0.01$ and $p \leq 0.001$, Fig. 6F), 2) nascent transcripts (FRNA) and NLIs ($p \leq 0.05$ and $p \leq 0.01$, Fig. 6G), and 3) transgene foci and nascent transcripts ($p \leq 0.05$ and $p \leq 0.001$, Fig. 6H). Moreover, the portion of NLIs colocalised simultaneously with transgene foci and nascent transcripts was 1.5 times higher upon transcription induction. We thus showed that the transcriptionally active foci and nascent RNA are preferentially positioned at the discrete NLIs.

Altogether, these data obtained using a transcriptionally inducible transgenic array and the pulse-labelling of nascent transcripts clearly demonstrate that active chromatin can dynamically re-associate with NLIs and that transcriptionally active genes are preferentially adjacent to the surface of NLIs.

Discussion

It is known that the transcription of multiple genes is clustered to form transcription factories (Misteli, 2007; Pombo et al., 1999; Xu and Cook, 2008). Nevertheless, how this compartmentalisation of transcription is achieved is unclear. In this study, we observed that nascent RNA transcripts, Pol II, and transcription factors TFIID, TFIIE, TFIIH associate with PtdIns(4,5)P_2 in the nucleus. Strikingly, we found that this nucleoplasmic PtdIns(4,5)P_2 is organised in 40–100-nm structures distinct from nuclear speckles and nucleoli, to which we referred as NLIs. Furthermore, we revealed that transcriptionally active transgene loci and ~43% of all nuclear nascent transcripts localise to NLIs, suggesting that a substantial portion of transcriptional activity occurs at the NLI periphery. Remarkably, we showed that PtdIns(4,5)P_2 hydrolysis results in a significant decrease of the transcription level in the NLI area. We hypothesise that these NLIs might serve as a structural platform which facilitates the functioning of Pol II transcription factories. Our hypothesis is supported by the fact that nuclear PtdIns(4,5)P_2 is highly resistant to detergent extraction, most probably due to its involvement in larger complexes (Gonzales and Anderson, 2006; Vann et al., 1997). Moreover, we revealed that neither DNase treatment nor the inhibition of Pol II transcription affects NLIs. NLIs are thus abundant nuclear domains stably present in the nucleoplasm being structurally independent of ongoing transcription.

Next, we addressed the issue of how the transcription complexes are associated with NLI periphery. Our results document that NLIs are chromatin-independent structures and a DNA template does not mediate the interaction between NLIs and Pol II transcription machinery. On the contrary, RNase treatment disrupts NLIs. In accordance with this, the majority of NLIs colocalise with RNA detected by RNase-gold. The RNase-gold complex recognises total RNA, a part of which can be represented by nascent RNA transcripts. Recently, the role for Neat 1, Sat III, and Malat 1 noncoding RNAs (ncRNAs) in the recruitment and assembly of core paraspeckle proteins, nuclear stress body proteins, and splicing factors, respectively, was shown (Mao et al., 2011; Shevtsov and Dundr, 2011; Tripathi et al., 2012). In addition, asFGFR2 long ncRNA was shown to recruit chromatin modifiers to a gene, which impaired the binding of the splicing repressor, thus creating an interface between DNA, chromatin remodellers, histone demethylases, mRNA, and splicing factors (Gonzalez et al., 2015). That is why we hypothesise that not only nascent RNA transcripts but also other types of RNA such as ncRNAs might mediate the interaction between NLIs and transcription complexes.

RNA itself is unlikely to serve as a mediator, because the negative charges of PtdIns(4,5)P_2 hydrophilic heads exposed to the surface of the islets would repulse negatively charged RNA. Therefore, NLIs and RNA molecules should have some positively charged interface, presumably the basic protein domains. It was recently shown that the binding between LINK-A long ncRNA and PtdIns(3,4,5)P_3 promotes the association of the PH domain of serine/threonine-specific protein kinase AKT with PtdIns(3,4,5)P_3, leading to AKT phosphorylation and activation (Lin et al., 2017). Here we

show that NLIs interact with NM1. It is known that the C-terminal part of NM1 containing the PtdIns(4,5)P_2-binding site is essential for NM1 to promote chromatin remodelling and Pol II transcription (Almuzzaini et al., 2015; Hofmann et al., 2006). We revealed that K908A mutation in NM1 causes a loss of interaction with Pol II. Furthermore, NM1(K908A) is incapable to rescue the drop in transcription caused by the knock-down of endogenous NM1. Therefore, we speculate that the interaction between NM1 and the Pol II complex occurs via PtdIns(4,5)P_2 at the periphery of NLIs. In such a way, NM1 can recruit chromatin-remodelling complexes to NLIs, where the remodellers are able to create an open chromatin structure, thus promoting transcription. In the absence of NM1–NLI association, Pol II complexes can remain attached to the surface of NLIs, but transcription cannot occur due to the lack of chromatin remodellers. Additionally, due to its basic nature, NM1 is able to create an interface between negatively charged PtdIns(4,5)P_2 and RNA.

Recently, other lipid-based structures – nuclear lipid droplets (nLDs), which might indirectly participate in transcription via nuclear lipid metabolism, were described (Layerenza et al., 2013; Ohsaki et al., 2016; Uzbekov and Roingeard, 2013). nLDs were shown to consist of a hydrophobic lipid core surrounded by a hydrophilic outer monolayer (Layerenza et al., 2013). In the inner part of nLDs, triacylglycerols and cholesteryl esters were found, whereas polar lipids, cholesterol, and proteins form their surface. Despite being very different from them, NLIs appear to be organised in a similar way with a carbon-rich interior and phosphorus- and nitrogen-rich exterior. Thus we infer that the inner core of NLIs is composed of lipids, while PtdIns(4,5)P_2 molecules form the outer layer with hydrophilic heads facing outwards enclosed by nucleic acids and proteins. Our hypothesis is supported by the specific association of PtdIns(4,5)P_2 with phosphatidylcholines, phosphatidylethanolamines, triacylglycerols, and sphingomyelins, shown in this study. However, NLIs and nLDs differ in a number of parameters. A comparison between the TEM of nLDs (Ohsaki et al., 2016; Uzbekov and Roingeard, 2013) and the TEM of NLIs (this study) clearly shows their ultrastructural dissimilarities: nLDs are about ten times larger than NLIs, are characterised by homogeneous interior distinguishable from the surrounding nucleoplasm, and have contacts with the extensions of the inner nuclear membrane. Moreover, nLDs were observed in rat and human hepatocarcinoma cells, U2OS cells, and mouse hepatocytes only, while they were rare in HeLa cells and human fibroblasts (Ohsaki et al., 2016). In contrast, we found NLIs not only in human cancer cells (HeLa, U2OS), but also in normal human fibroblasts as well as in yeast, protozoan, plant, and animal cells, and they are ultrastructurally identical (data not shown). This evolutionary conservation indicates that NLIs are common structures essential for nuclear processes regardless of cell type. In support of this notion, it was shown that inositol polyphosphates Ins(1,3,4,5)P_4 and Ins(1,3,4,5,6)P_5, synthesised from PtdIns(4,5)P_2, stimulate the mobilisation of nucleosomes by the yeast SWI/SNF complex affecting chromatin remodelling and gene expression (Shen et al., 2003). In protozoa, PtdIns(4,5)P_2 serves as a substrate for phosphatidylinositol-4,5-bisphosphate 3-kinase, which is implicated in the macronuclear division mediated by microtubules (Smith et al., 2004). As regards

plants, the negative effect of increased nuclear level of PtdIns(4,5)P_2 on DNA synthesis, histone H3K9 acetylation, and the phosphorylation of the retinoblastoma protein was shown in tobacco cells (Dieck et al., 2012). On the other hand, heat stress caused PtdIns(4,5)P_2 accumulation in the nuclear sub-compartments in tobacco, arabidopsis, and rice plants, which is considered as a part of the complex response implicating transcriptional and post-transcriptional changes (Mishkind et al., 2009).

In addition, nLDs serve as a storage nuclear domain for lipids (Layerenza et al., 2013) and harbour the enzymes of triglyceride and phosphatidylcholine synthesis, thus they may regulate the local concentrations of fatty acids in the nucleus (Ohsaki et al., 2016). NLIs might be the storage sites for PtdIns(4,5)P_2 as well, however our results strongly indicate rather their involvement in RNA synthesis.

Apart from nLDs, some other nuclear lipid-containing structures have been described. It was shown that sphingomyelin and nascent RNA are both located in the transcriptionally active chromatin regions in rat and mouse liver cells, T24 human bladder carcinoma cells, and V79 Chinese hamster cells (Scassellati et al., 2010). The rat hepatocyte intranuclear complexes (ICs) containing the STAT3 transcription factor, phosphatidylcholine, sphingomyelin, cholesterol, ceramide, and newly synthesised double-stranded RNA (dsRNA) were described (Micheli et al., 1998; Rossi et al., 2007a; Rossi et al., 2007b). The authors proposed a role for ICs in the regulation of cell proliferation and retention of nuclear dsRNA. Unlike, NLIs do not have (only) dsRNA because RNase treatment results in their loss.

Until now, the only known nuclear subcompartments containing PtdIns(4,5)P_2 were nucleoplasmic vesicles, which serve as the storage nuclear domain for calcium and might be involved in transcription via calcium-regulated chromatin remodelling in bovine adrenal chromaffin cells (Yoo et al., 2014). Even though similar to NLIs in size (50 nm), these vesicles are enclosed by a membrane. On the contrary, NLIs have no discernible membrane as we definitely showed by the electron microscopy experiments.

Furthermore, we found cholesterol and ceramide at the periphery of NLIs. We suggest that PtdIns(4,5)P_2, cholesterol, and ceramide may contribute to the formation of the interface between NLIs and the surrounding nucleoplasm. In such a way, NLIs may acquire the properties of a phase-separated system (Brangwynne et al., 2011; Feric et al., 2016; Iborra, 2007; Jost et al., 2014; Richter et al., 2008; Strom et al., 2017), thus facilitating the assembly of lipids, proteins, and nucleic acids and functioning as small reaction compartments.

It is still unclear how the actively transcribed DNA loci are compartmentalised in the nuclear volume (Bickmore and van Steensel, 2013). We hypothesise that NLIs, due to their lipidic nature with a hydrophilic coat, have a role in the spatial formation and maintenance of transcription factories and they thus participate in nuclear organisation.

In conclusion, we described a novel nuclear structure – NLIs, which are important for ongoing Pol II transcription. Future experiments will clarify the composition of the inner hydrophobic core of NLIs and determine why their surface is important for active transcription and whether there is some specialisation between NLIs and interacting genomic elements as suggested by the heterogeneity in the composition of NLIs. All the findings described here as well as future studies will undoubtedly contribute to the understanding of the role of these structures in the global nuclear architecture and the modulation of transcriptional patterns in cells.

Materials and methods

Cell cultures and transfections

Human cervical carcinoma (HeLa, ATCC No. CCL2) cells, human osteosarcoma (U2OS, ATCC No. HTB96) cells, and human lung carcinoma H1299 (ATCC No. CRL5803) cells were grown in D-MEM with 10% fetal bovine serum (FBS) at +37°C in humidified 5% CO_2 atmosphere. Suspension HeLa cells were kept in S-MEM supplemented with 5% FBS at +37°C in humidified 5% CO_2 atmosphere. Transfections were carried out using Lipofectamine 2000 (Invitrogen, Thermo Fisher Scientific, Waltham, MA, USA) according to the manufacturer's protocol. Stable cell lines were prepared by lentiviral transduction using packaging plasmids psPAX and pMD2.G (Addgene, Didier Trono lab, Cambridge, MA, USA). U2OS 2-6-3 cells stably expressing the p3216PECMS2β plasmid were received from Dr Susan Janicki.

Constructs

Nuclear myosin 1 (NM1)-flag and NM1(K908A)-flag: the cDNAs of NM1 and NM1(K908A) were C-terminally fused with a flag tag and cloned into a lentiviral expression vector pCDH-CMV-MCS-EF1-Neo (System Biosciences, Palo Alto, CA, USA) using EcorI and BamHI. The K908A mutant was obtained by site-directed mutagenesis. Flag-HDL: the cDNA fragment of NM1 (corresponding to amino acids 712–1044) was amplified by PCR, fused with an N-terminal flag tag and ligated into pCDNA3.1 (Invitrogen, Thermo Fisher Scientific, Waltham, MA, USA) using SacI and XmaI. NM1 shRNA: NM1 shRNA, targeting the sequence 5'-gcccgtccagtatttcaac-3' (Open Biosystems, Dharmacon, Inc., Lafayette, CO, USA; No TRCN0000122925 AAO75-C-8), was ligated into pLKO.1 (Addgene, Didier Trono lab, Cambridge, MA, USA) according to (Stewart et al., 2003). His-tagged 1-phosphatidylinositol-4,5-bisphosphate phosphodiesterase delta-1 (PLC) and the PtdIns(4,5)P_2-binding mutant R40A (PLC(R40A) in pRSETA were both generous gifts from Dr Hitoshi Yagisawa and Dr Klim King (Cheng et al., 1995). The GST-tagged PLC PH domain was as described (Fujita et al., 2009). pSV2-EYFP-LacI was a kind gift from Dr David Spector. pLVX-Tet-On Advanced was from Clontech Laboratories, Inc. (Mountain View, CA, USA).

The expression and purification of recombinant proteins

NM1-flag and NM1(K908A)-flag were stably expressed in the H1299 cell line. The cells were washed with PBS and extracted with lysis buffer (50 mM HEPES pH 8, 300 mM NaCl, 4 mM $MgCl_2$, 1% Triton X-100). The extract was sonicated, filtered through a 0.45-µm filter, and incubated for 2 h with pre-equilibrated anti-flag-M2 agarose beads (Sigma-Aldrich, Merck KGaA, St. Louis, MO,

USA). The beads were then washed three times with lysis buffer, and bound proteins were eluted five times with 100 µg/ml flag peptide in elution buffer (10 mM Tris pH 8, 100 mM NaCl, 0.5% EDTA, 20% glycerol). His-tagged PLC and PLC(R40A) were expressed in *E. coli* strain BL21-Gold (Agilent Technologies, Santa Clara, CA, USA) and purified over a Ni-NTA column as described previously (Cheng et al., 1995). The GST-tagged PLC PH domain was expressed and purified as described (Fujita et al., 2009).

Immunofluorescent labelling for super-resolution structured illumination microscopy (SIM).

Cells grown on high-performance cover glasses of 18x18 mm² with restricted thickness-related tolerance D=0.17 mm +/- 0.005 mm and the refractive index = 1.5255 +/- 0.0015 were fixed with 3% formaldehyde and permeabilised with 0.1% Triton X-100. Unspecific targets were blocked with 0.25% bovine serum albumin (BSA) with 0.25% gelatine. All solutions were diluted in PBS. Then, the cells were incubated with primary antibodies diluted in PBS, secondary antibodies diluted in PBS or PBST, stained with DAPI and mounted in Mowiol. Importantly for the super-resolution microscopy technique, five extensive washes in PBS or PBST were done for 5 or 10 min between each of the steps.

DNase and RNase treatments

U2OS cells were gently fixed on ice with 1% formaldehyde for 5 min and then treated with either RNase A (1 mg/ml) or DNase I (250 U/ml) diluted in a buffer (130 mM KCl, 10 mM Na_2HPO4, 1 mM $MgCl_2$, 1 mM DTT, 1 mM Na_2ATP, 0.1 mM PMSF; pH 7.4) at 32°C for 30 min. Subsequently, the cells were fixed, permeabilised, and further processed for SIM as described above.

BrU labelling of nascent transcripts for SIM and transmission electron microscopy (TEM)

HeLa cells were washed in a PB buffer on ice (100 mM CH_3COOK, 30 mM KCl, 10 mM Na_2HPO4, 1 mM $MgCl_2$, 1 mM DTT, 0.2 mM PMSF, 10 U/ml human placental RNase inhibitor (HPRI), 1 mM Na_2ATP; pH 7.2) and permeabilised with 0.5 mg/ml saponin on ice for 5 min. Transcription reactions were started by incubation with 100 µM BrUTP, 100 µM CTP, 100 µM GTP, and 300 µM $MgCl_2$ in PB. To inhibit Pol II transcription, cells were pre-incubated with 100 µg/ml α-amanitin for 5 min. After 15 min at 35°C, the reactions were stopped by rinsing in ice-cold PB. The cells were either fixed with 4% formaldehyde on ice for 40 min, additionally permeabilised with 0.5% Triton X-100 for 20 min, and further processed for SIM as described above or processed for TEM (Sobol et al., 2010).

SIM

The images were acquired using an ECLIPSE Ti-E microscope equipped with an Andor iXon3 897 EMCCD camera with a CFI SR Apochromat TIRF 100x/1.49 oil objective (Nikon Corporation, Tokyo, Japan). NIS-Elements AR 4.20.01 and NIS Elements AR 4.30 software was used for image capture and analysis. In each experiment, the images of all samples were acquired and reconstructed with the same parameters to ensure their comparability. To assess the distribution of PtdIns(4,5)P_2 in the nucleus, z-stack was acquired, reconstructed, and analysed using the 3D Object Measurement tool. We defined the nucleus with DAPI and histone H1, and the nucleoli as the regions, where both markers were absent. Nuclear speckles were distinguished from nuclear lipid islets (NLIs) based on the co-labelling with a speckle-specific marker, Son. All markers were visualised with different secondary antibodies than PtdIns(4,5)P_2. The respective volumes of nuclear speckles, NLIs, and nucleolar PtdIns(4,5)P_2 were calculated. To determine the proper threshold, MATLAB 7.7.0 (R2008b) software was used. Firstly, the maximum intensity value for each pixel in the projection image was computed as the maximum value of the overlapping voxels in z-stack (PtdIns(4,5)P_2 channel). Secondly, the upper quartile was applied to filter out 75% of non-significant pixel intensities of the projection image. The zero intensity values were assigned to all of these pixels, which have the intensity value lower than the given upper quartile, so that they are considered as a black background or noise. Consequently, the projection image in the PtdIns(4,5)P_2 channel includes 25% of the intensity values of the original projection image. The image was colour-coded in red. Simultaneously, the same method was applied to z-stack in Son, H1, and DAPI channels. The ninth decile was chosen to sort out non-significant intensity values in the projection image in Son channel. The zero values were assigned to all pixels with intensity values below the 90th percentile. In the next step, the projection images (PtdIns(4,5)P_2 channel and Son channel) were combined. All overlapping pixels with non-zero values in both channels were classified as nuclear speckles in the PtdIns(4,5)P_2 channel and colour-coded yellow. Then, the information on the maximum projection images of H1 and DAPI channels was used to distinguish the nucleoli in the PtdIns(4,5)P_2 channel, and classified pixels were colour-coded blue. The data on the volumes were exported and the percentage distribution of PtdIns(4,5)P_2 in the nucleus was calculated and presented as a diagram using Microsoft Excel software.

The colocalisation analysis of the SIM images from the experiment on co-labelling PtdIns(4,5)P_2, nascent RNA transcripts (BrRNA), the TATA-box binding protein (TBP) of the Pol II transcription factor TFIID (TFIID TBP), and the C-terminal domain of the Pol II largest subunit (Pol II CTD) was carried out using the free Fiji software package (https://fiji.sc/) and the JACoP plugin (http://imagejdocu.tudor.lu/doku.php?id=plugin:analysis:jacop_2.0:just_another_colocalization_plugin:start); a total of eight cells were analysed. To analyse the colocalisation between TFIID TBP, Pol II CTD, BrRNA, and each NLI taken separately, we simplified the processing of multiple images by

applying the simple custom-made macros created in Fiji. Shortly, the images were enhanced to obtain better visualisation of NLIs, but the values of their pixels were not changed. The image in the PtdIns(4,5)P_2 channel was automatically pre-segmented by finding the maximum intensity pixels of NLIs for the next easy segmentation (Fiji/Find Maxima plugin). The exact manual segmentation of NLIs was done by the Fiji/Blow-Lasso Tool plugin. The same region of interest found was applied to BrRNA or TFIID TBP, or Pol II CTD channels. This resulted in two segmented images from two different channels. All segmented pairs of images were statistically analysed. Quantitative results are presented in graphs as the mean ± standard deviation (s.d.). Statistical significance was determined using the F-test two-sample for variances, followed by the t-test: two-sample assuming (un-)equal variances. Prism 5 for Windows (version 5.04) was used to make all graphs presented in this study.

The visualisation of gene expression and immunofluorescent labelling followed by super-resolution stimulated emission depletion (STED) microscopy

U2OS 2-6-3 cells stably expressing a plasmid containing a *lac* operator (LacO), tetracycline response elements, a CMV minimal promoter, and CFP with peroxisomal targeting signal-1 [Ser-Lys-Leu (SKL)] (Janicki et al., 2004) were grown on high-performance cover glasses of d = 12 mm with restricted thickness-related tolerance D=0.17 mm +/- 0.005 mm and the refractive index = 1.5255 +/- 0.0015. The cells were co-transfected with the tetracycline-controlled transactivator (pLVX-Tet-On Advanced) and the EYFP-lac repressor (pSV2-EYFP-LacI). Transcription was induced by the addition of doxycycline to the medium. Then, fluorouridine (FU) was added to the final 2 mM and the cells were incubated for 30 min. The cells were fixed with 4% formaldehyde and permeabilised with 0.1% Triton X-100. Non-specific targets were blocked with 5% normal goat serum. All solutions were diluted in PBS. Then, the cells were incubated with anti-BrdU antibody to detect FU incorporated into the nascent RNA transcripts and anti-PtdIns(4,5)P_2 antibody, all diluted in PBS, secondary antibodies diluted in PBST, and mounted in 90% glycerol with 2.5% DABCO. Importantly for the super-resolution microscopy technique, five extensive washes in PBS or PBST were done for 5 or 10 min between each of the steps.

STED

The images were acquired using a Leica TCS SP8 STED 3X microscope equipped with a Leica DFC365 FX digital camera with a STED white CS 100x/1.40 oil objective for optimised overlay of excitation and a STED beam (Leica Mikrosysteme Vertrieb GmbH, Wetzlar, Germany). Image capture and analysis were done using the Leica LAS x64 bit software package with LAS AF SP8 Dye Finder, 3D visualisation, deconvolution and colocalisation module. The acquired image z-stacks were deconvolved using Huygens Professional software. The colocalisation analysis was carried out using

the free Fiji software package and the JACoP plugin. Approximately ten cells were analysed for each condition. To analyse the colocalisation between the transgene locus, nascent transcripts (FRNA), and each NLI taken separately, we simplified the processing of multiple images by applying the simple custom-made macros created in Fiji. Shortly, the images were enhanced to obtain better visualisation of NLIs, but the values of their pixels were not changed. The image in the PtdIns(4,5)P_2 channel was automatically pre-segmented by finding the maximum intensity pixels of NLIs for the next easy segmentation (Fiji/Find Maxima plugin). The exact manual segmentation of NLIs was done by the Fiji/Blow-Lasso Tool plugin. The same region of interest found was applied to LacO or FRNA channels. This resulted in two segmented images from two different channels. All segmented pairs of images were statistically analysed. The same procedure was applied for the analysis of colocalisation between Son, Aurora B kinase, and each NLI taken separately as well as for each nuclear speckle labelled by PtdIns(4,5)P_2 and Son. Eight cells were analysed for each pair: Son and PtdIns(4,5)P_2, Aurora B kinase and PtdIns(4,5)P_2.

Quantitative results are presented in graphs as the mean ± s.d. Statistical significance was determined using the F-test two-sample for variances, followed by the t-test: two-sample assuming (un-)equal variances.

The quantification of transcription using FU labelling of transcripts

U2OS cells, grown on cover glasses of d = 12 mm, were permeabilised with 0.05% Triton X-100 on ice for 5 min and then treated with recombinant PLC (84 µg/ml in the buffer consisting of 50 mM HEPES pH7.4, 100 mM KCl) and 0.04 µg/ml actinomycin D (AMD) as an inhibitor of Pol I transcription at RT for 1 h. After 30 min of treatment, FU was added to the final 2 mM and the cells were incubated for 30 min. Then the cells were washed, fixed with 4% formaldehyde and permeabilised with 0.1% Triton X-100. Unspecific targets were blocked with 5% normal goat serum. All solutions were diluted in PBS. Then, the cells were incubated with primary antibodies diluted in PBS, secondary antibodies diluted in PBST, stained with DAPI and mounted in ProlongGold. As the controls, buffer only or mutated PLC(R40A), or BSA, or PLC inactivated by heating were used. The images were acquired using an IX81 high-throughput wide-field microscope with an UPLSAPO 40x/0.90 oil objective (Olympus Corporation, Tokyo, Japan). SCAN-R automated image and data analysis software was used for image capture and analysis. The images were captured as 1 µm z-stacks with a 200 nm z-step. For the analysis, the DAPI channel was used to determine the nuclear area and the Son channel was used to determine the nuclear speckle area. The total fluorescence intensity was calculated from the maximum projection image for each z-stack in the PtdIns(4,5)P_2 channel and the FU channel separately. In summary, 915 control cells, 830 cells treated with mutated PLC(R40A), 920 cells treated with PLC inactivated by heating, 398 cells treated with BSA, and 854 cells treated with PLC were analysed. Fluorescence intensity in each channel and the area of NLIs

were calculated as a result of the subtraction of the corresponding parameter for nuclear speckles from the same parameter for the whole nucleus. Results from two independent experiments are presented as the intensity of fluorescence per unit area in percent to control value (the mean ± s.d.). Statistical significance was determined using the F-test two-sample for variances, followed by the t-test: two-sample assuming (un-)equal variances.

H1299 cells were treated with 0.04 μg/ml AMD for 1 h. After 30 min of treatment, the cells were incubated with 2 mM FU for 30 min. After this time period, the cells were washed, fixed, and permeabilised. FU incorporated into nascent transcripts was detected using anti-BrdU antibody, and fluorescence intensity was measured, quantified, analysed, and presented as described above. In summary, 1677 cells transfected with control shRNA, 2219 cells transfected with NM1 shRNA, 1930 cells transfected with NM1 shRNA and NM1-flag, and 1322 cells transfected with NM1 shRNA and NM1(K908A)-flag were analysed.

TEM

HeLa cells were fixed in 3% formaldehyde with 0.1% glutaraldehyde and embedded into LR White resin or Lowicryl K4M resin using a standard protocol (Sobol et al., 2010; Wright, 2000). Alternatively, HeLa cells were high-pressure frozen, freeze-substituted and embedded into LR White resin or Lowicryl K4M resin according to a previously published procedure (Sobol et al., 2011). Ultrathin sections (70 nm) were immunolabelled by a conventional protocol (Stradalova et al., 2008) and examined with a Morgagni 268 transmission electron microscope (TEM) at 80 kV and a Tecnai G2 20 LaB6 TEM at 200 kV (both from FEI, Eindhoven, the Netherlands). The images were captured with a Mega View III CCD camera and a Gatan Model 894 UltraScan 1000 camera. Multiple sections of repetitive immunogold labelling experiments were analysed. To facilitate the visualisation of 6 nm gold nanoparticles in images, Adobe Photoshop CS3 Version 10.0 was used to cover the small nanoparticles co-centrically with red dots. To evaluate computationally the spatial distribution and quantitative mutual dependence of the nanoparticles in electron microscopy images, we developed and used the quantitative objective approach (Pastorek et al., 2016), based on the previously published one describing pair cross-correlation function – PCCF (Philimonenko et al., 2000). In this study, we used a newly developed plugin (Pastorek et al., 2016) on the Fiji software platform to quantify the relative colocalisation coefficient – RCC. In summary, we analysed 21 cells co-labelled for NM1 and PtdIns(4,5)P_2; 59 control cells and 213 α-amanitin-treated cells co-labelled for BrRNA and PtdIns(4,5)P_2; 37 cells co-labelled for RNA and PtdIns(4,5)P_2; 20 cells co-labelled for cholesterol and PtdIns(4,5)P_2, and 41 cells co-labelled for ceramide and PtdIns(4,5)P_2. Quantitative results are presented in graphs as the mean ± s.d. Statistical significance was determined using the F-test two-sample for variances, followed by the t-test: two-sample assuming (un-)equal variances.

Electron energy loss spectroscopy (EELS) and elemental mapping

Elemental mapping was performed on ultrathin sections of U2OS cells embedded in LR White resin. The 80-nm sections were immunolabelled with anti-PtdIns(4,5)P_2 antibody and secondary antibody conjugated with 12 nm gold particles according to a conventional protocol (Stradalova et al., 2008). Contrasting by uranyl acetate was omitted. EELS mapping of the distribution of specific elements was performed using Tecnai G2 20 LaB6 TEM at 200 kV equipped with a Gatan 863 Tridiem Imaging Filter. Two pre-edge and one post-edge energy-filtered images were collected at 100 eV, 120 eV, and 152 eV ($L_{II,\ III}$ edge) for phosphorus; at 353 eV, 383 eV, and 416 eV (K edge) for nitrogen; at 484 eV, 514 eV, and 532 eV (K edge) for oxygen; at 130 eV, 150 eV, and 165 eV ($L_{II,\ III}$ edge) for sulphur; at 252 eV, 272 eV, and at 294 eV (K edge) for carbon. Drift correction was performed using an automated statistically determined spatial drift (SDSD) correction script for Digital Micrograph (Schaffer et al., 2004), and elemental maps were calculated by the three-window method using Digital Micrograph. The images were processed using Digital Micrograph and Adobe Photoshop CS3 Version 10.0.

Ultrastructural detection of RNA molecules using RNase-gold

RNase A (Thermo Fisher Scientific, Waltham, MA, USA) was conjugated with 10 nm gold nanoparticles (BBI Solutions, Cardiff, UK) as published previously (Bendayan, 1981; Bendayan and Puvion, 1984; Cheniclet and Bendayan, 1990). HeLa cells were embedded into Lowicryl K4M resin and the ultrathin sections (70 nm) were sequentially double-labelled. First, the anti-PtdIns(4,5)P_2 antibody followed by the secondary antibody conjugated with 6 nm gold nanoparticles was applied. Next, the sections were incubated with RNase-gold conjugates (0.08 µg/ml). The activity of the RNase-gold complex was checked using an *in vitro* reaction with RNA (0.5 µg of RNA for 18 ng of RNase-gold). The incubation was carried out on ice for 15 min. To control the labelling specificity, the RNase-gold complex (3.2 ng) was pre-blocked with RNA (5.2–20.0 µg), and these mixtures were used for labelling.

Quick-freezing and freeze-fracture replica labelling (QF-FRL)

HeLa cells were pelleted, placed onto a disc for high-pressure freezing, covered with a thin foil and frozen in a HPM 010 high-pressure freezing machine (Bal-Tec A.G., Balzers, Liechtenstein). The specimens were then transferred to a cold stage of a Balzers BAF400 apparatus and freeze-fractured at a temperature ranging from -105°C to -120°C at a pressure of $2x10^{-6}$ mbar. Replicas were made by electron-beam evaporation of platinum (Pt)/carbon (C) and C. Finally, the fractured cells were coated by a 2-nm C layer followed by a 2-nm Pt/C layer and then by a 20-nm C layer. The replica thickness

was controlled using a crystal thickness monitor. After thawing, the replicas of cells were digested by 2.5% SDS in PBS at +60ºC overnight. The replicas were kept in 50% glycerol at -20ºC until labelling. For labelling, the replicas were rinsed with 1% Triton X-100 in PBS or PBST, blocked with 3% BSA plus 2% cold fish gelatine in PBS for 30 min and incubated in primary antibody diluted with 1% BSA in PBST at +4ºC overnight. Then the replicas were incubated in secondary antibody conjugated with gold nanoparticles diluted using 1% BSA in PBS at +37ºC for 30 min. Alternatively, the replicas were incubated with the GST-tagged PLC PH domain and anti-ceramide antibody, both diluted in 1% BSA plus 1% cold fish gelatine in PBST, at +4ºC overnight. Then the replicas were incubated with anti-GST antibody and anti-ceramide antibody, followed by the incubation with protein A conjugated with 10 nm gold nanoparticles and secondary antibody conjugated with 6 nm gold nanoparticles, both diluted with 1% BSA in PBS at +37ºC for 30 min. The replicas were rinsed with 0.1% BSA in PBST between each of the incubations. Finally, the replicas were rinsed with distilled water and picked up on the formvar-coated copper grids. The specimens were observed with a JEOL1010 TEM electron microscope.

PIP strip

Membranes spotted with phosphoinositides and lipids (PIP strips; Echelon Biosciences, Inc., Salt Lake City, UT, USA) were blocked with 3% BSA in PBST at +4°C for 1 h. Recombinant NM1-flag and NM1(K908A)-flag were diluted to 2 µg/ml with 3% BSA in PBST and incubated with PIP strips at +4°C for 4 h. After five washes with PBST, bound proteins were detected by western blotting with anti-flag antibody.

Nuclear extract fractionation and dot blot analysis

HeLa nuclear extracts were fractionated by the discontinuous sucrose gradient ultracentrifugation method, adapted from (Marmor and Julius, 2001). Nuclei from suspension HeLa cells were prepared as described previously (Trinkle-Mulcahy et al., 2008). Clean nuclei were extracted by TKM buffer (50 mM Tris pH 7.4, 25 mM KCl, 5 mM $MgCl_2$, 1 mM EDTA, 0.5% Brij 98, EDTA-free protease inhibitor), sonicated 3x10 sec on ice, and centrifuged at 16,000 g for 5 min. 250 µl of nuclear extract were mixed with the same amount of 80% sucrose in TKM buffer and placed at the bottom of the tube. Samples were sequentially overlaid with 4.3 ml of 36% and 0.2 ml of 5% sucrose solution to a total volume of 5 ml. The mixture was subjected to equilibrium density gradient centrifugation at 50000 rpm in a MLS50 rotor (Beckman Coulter, Fullerton, CA, USA) at +4°C for 18 h. 200 µl from each of the collected fractions were spotted on a nitrocellulose membrane and probed for

PtdIns(4,5)P_2. To identify the protein composition, 20 µl of each fraction were resolved by SDS-PAGE, transferred onto a nitrocellulose membrane and immunoprobed with the respective antibody.

A pull-down assay and co-immunoprecipitation

Nuclei from suspension HeLa cells were prepared as described previously (Trinkle-Mulcahy et al., 2008). Pure nuclei were extracted using RIPA buffer (50 mM Tris pH 8, 150 mM NaCl, 0.5% NP-40, complete protease inhibitors from F. Hoffmann-La Roche Ltd., Basel, Switzerland), sonicated and spun at 16,000 g for 15 min. The clear lysate was incubated with pre-equilibrated PtdIns(4,5)P_2-coated agarose beads (Echelon Biosciences, Inc., Salt Lake City, UT, USA) for 2 h at +4°C. Beads were then washed three times with RIPA. Alternatively, nuclei were prepared by Lamond Lab Protocol 2007 (http://www.trinklelab.com/pubpdf/CellFractionation.pdf), extracted using RIPA buffer (50 mM Tris pH 7.5, 150 mM NaCl, 1% NP-40, complete protease inhibitors from F. Hoffmann-La Roche Ltd., Basel, Switzerland), sonicated, and centrifuged at 16,100 g for 10 min. The cleared lysate was incubated with the anti-PtdIns(4,5)P_2 antibody or with the isotype control antibody at +4°C overnight. Then the lysate was incubated with L-protein magnetic beads at +4°C for 1 h. Bound proteins were eluted by boiling in Laemmli buffer, separated by SDS-PAGE, and detected by subsequent immunoblotting.

H1299 stable cell lines were lysed in lysis buffer (20 mM HEPES pH 8, 150 mM NaCl, 0.5% Triton X-100, complete protease inhibitors and PhosStop phosphatase inhibitors – both from F. Hoffmann-La Roche Ltd., Basel, Switzerland). The lysate was sonicated and cleared by centrifugation at 16,000 g for 15 min. The clear lysate was incubated with pre-equilibrated anti-flag-M2 agarose beads (Sigma-Aldrich, Merck KGaA, St. Louis, MO, USA) for 2 h. After three washes with lysis buffer, bound proteins were processed as described above.

Immunoprecipitation for lipid analysis

HeLa suspension cells were lysed in lysis buffer (50 mM HEPES pH 7.4. 150 mM NaCl, 1% NP-40, complete protease inhibitors from F. Hoffmann-La Roche Ltd., Basel, Switzerland) and nuclei were pelleted at 3000 g for 10 min. Then pure nuclei were resuspended in lysis buffer, sonicated, and centrifuged at 5,000 g for 20 min. The cleared nuclear fraction was incubated with Bio-Beads SM-2 Resin (Bio-Rad Laboratories, Inc., Hercules, CA, USA; 400 mg of the resin per 2 mg of protein) to adsorb the detergent NP-40, which can interfere with the following lipid analysis, at +4°C for 2 h. The cleared nuclear fraction was then aspirated and incubated at +4°C for 2 h with magnetic tosylactivated MyOne beads (Thermo Fisher Scientific, Waltham, MA, USA), preliminarily coupled with the anti-PtdIns(4,5)P_2 antibody or with the isotype control antibody at +4°C overnight (100 µl of beads per 5

µg of antibody per 1 mg of protein). Beads with immunoprecipitates were washed five times with wash buffer (10 mM HEPES 7.9, 150 mM NaCl) and processed for lipid analysis.

Lipid analysis

The chemicals used were as follows. The LC/MS grade acetonitrile and methanol (Sigma-Aldrich, Merck KGaA, St. Louis, MO, USA) were used as received; chloroform was distilled in glass from analytical-grade solvent. The internal standard 1,2-dilauroyl-*sn*-glycero-3-phosphoethanolamine (PE(12:0/12:0)) was purchased from Cayman Chemical (Ann Arbor, MI, USA). The standards of polar lipids used for the identification of lipid classes (phosphatidylethanolamines (PE), sphingomyelins (SM), phosphatidylcholines (PC), and lysophosphatidylcholines (LPC)) were from Matreya LLC (Pleasant Gap, PA, USA).

Lipid extraction from immunoprecipitates was done as follows. Water suspension of beads with immunoprecipitates was transferred from plastic tubes to glass vials. While the beads were being held in place, water was removed. Chloroform (100 µl), methanol (150 µl), and the internal standard solution (50 µl of 1,2-dilauroyl-*sn*-glycero-3-phosphoethanolamine, 0.1 µg/ml in methanol) were added to beads and the mixture was shaken for 8 min. The extract was transferred to a new glass vial, evaporated by a stream of nitrogen to dryness, and the residues were reconstituted in 25 µl of methanol:chloroform mixture (3:2 by volume).

Lipid extraction from the input nuclear fraction was done as follows. The sample (35–100 µl) was shaken for 30 min with 1 ml of methanol:chloroform (1:1 by volume), 50 µl of the internal standard solution (1,2-dilauroyl-sn-glycero-3-phosphoethanolamine, 0.1 µg/ml in methanol), and water (0.4 ml) in a glass vial. The mixture was centrifuged for 3 min to separate two layers. The chloroform layer was transferred into a new glass tube, the solvent was evaporated under a stream of nitrogen to dryness, and the residues were reconstituted in 25 µl of methanol:chloroform (3:2 by volume). The extracted lipids were stored at -20°C.

Hydrophilic interaction liquid chromatography – ultrahigh-performance liquid chromatography/electrospray ionisation – mass spectrometry (HILIC-UHPLC/ESI-MS) was done as follows. The liquid chromatograph consisted of a Rheos Alegro UHPLC pump, an Accela autosampler with column thermostat and an LCQ Fleet ion-trap mass spectrometer. The system was controlled by Xcalibur software (all by Thermo Fisher Scientific, Waltham, MA, USA). The HILIC-UHPLC/ESI-MS procedure with an Acquity UPLC HILIC column (50 mm × 2.1 mm, particle size: 1.7 µm; Waters) was modified from the original method (Holcapek et al., 2015). A column thermostat maintained the column temperature at +30°C and the injected volume of the samples was 5 µl. The flow rate of the mobile phase was 200 µl/min. The solvent gradient was programmed as follows: 0 min – 96% of A and 4% of B; 15 min – 70% of A and 30% of B, where A was acetonitrile and B was 10 mmol/l aqueous ammonium acetate. ESI in the positive ion mode was operated as follows: the

source voltage was 6 kV, sheath gas flow 40, aux gas flow 10, capillary voltage 17 V, capillary temperature +300°C, and tube lens voltage 95 V. Mass spectra were collected in the mass range of 200–1500 *m/z*. Lipids were identified based on their retention times and the *m/z* values of $[M+H]^+$ or $[M+NH_4]^+$ with the help of previously published data (Holcapek et al., 2015). The peak areas corresponding to lipid classes in the base-peak chromatogram (*m/z* 570–900) and the internal standard were used for quantification.

Antibodies

Primary antibodies: anti-β-actin mouse monoclonal IgG2a antibody (Sigma-Aldrich, Merck KGaA, St. Louis, MO, USA; A5316, clone AC-74; 0.24 µg/ml for western blot); anti-Aurora B rabbit polyclonal IgG antibody (Abcam, Cambridge, UK; ab2254; 1:200 for STED); anti-bromodeoxyuridine mouse IgG1 antibody (F. Hoffmann-La Roche Ltd., Basel, Switzerland; 11170376001, clone BMC9318; 4 µg/ml for SIM, 20 µg/ml for TEM); anti-bromodeoxyuridine mouse monoclonal IgG1 antibody (Sigma-Aldrich, Merck KGaA, St. Louis, MO, USA; B8434, clone BU-33; 17.6 µg/ml for STED and SCAN-R); anti-ceramide mouse monoclonal IgM antibody (Enzo Life Sciences, Inc., Farmingdale, NY, USA; ALX-804-196-T050; 1:10 for TEM); anti-cholesterol rabbit polyclonal IgG antibody (Cloud-Clone Corp., Katy, TX, USA; CPB701Ge21; 20 µg/ml for TEM); anti-flag mouse monoclonal IgG1 antibody (Sigma-Aldrich, Merck KGaA, St. Louis, MO, USA; F1804, clone M2; 0.4 µg/ml for western blot and 20 µg/ml for TEM); anti-GAPDH mouse monoclonal IgG3 antibody (Acris Antibodies GmbH, OriGene Company, Herford, Germany; clone 6G5; 0.22 µg/ml for western blot); anti-GST rabbit polyclonal IgG antibody (Abcam, Cambridge, UK; ab19256; 10 µg/ml for QF-FRL); anti-His mouse monoclonal IgG2a antibody (Sigma-Aldrich, Merck KGaA, St. Louis, MO, USA; H1029; 0.4 µg/ml for western blot); anti-histone H1 mouse monoclonal IgG2a antibody (Abcam, Cambridge, UK; ab71594, clone AE-4; 10 µg/ml for SIM); anti-H3K4me2 rabbit polyclonal IgG antibody (Merck Millipore, Merck KGaA, Burlington, MA, USA; 07-030; 1:300 for SIM); anti-H3K9me2 rabbit polyclonal IgG antibody (Merck Millipore, Merck KGaA, Burlington, MA, USA; 17-648; 1:300 for SIM); isotype control mouse monoclonal IgM antibody (Abcam, Cambridge, UK; ab18400, clone MM-30; 2.72 µg per 1 mg of protein for co-IP, 5 µg per 1 mg of protein for IP); anti-lamin A/C mouse monoclonal IgG antibody (a gift from C.J. Hutchison; clone JOL2; 1:500 for western blot); anti-NM1 rabbit polyclonal IgG antibody (Sigma-Aldrich, Merck KGaA, St. Louis, MO, USA; M3567; 1 µg/ml for western blot); anti-PtdIns(4,5)P_2 mouse monoclonal IgM antibody (Abcam, Cambridge, UK; clone 2C11; 2 µg/ml for dot blot); anti-PtdIns(4,5)P_2 mouse monoclonal IgM antibody (Echelon Biosciences, Inc., Salt Lake City, UT, USA; Z-A045, clone 2C11; 5-10 µg/ml for SIM, 3 µg/ml for STED and SCAN-R, 10 µg/ml for TEM, 2.72 µg per 1 mg of protein for co-IP, 5 µg per 1 mg of protein for IP); anti-RNA Pol II CTD mouse monoclonal IgG2/K antibody (a gift from Prof. Primal de Lanerolle; clone 8WG16; 1:2000 for

western blot), anti-RNA Pol II CTD rabbit polyclonal IgG antibody (Abcam, Cambridge, UK; ab26721; 6 µg/ml for SIM, 1.2 µg/ml for western blot); anti-RNA Pol II CTD S2 rabbit polyclonal IgG antibody (Abcam, Cambridge, UK; ab24758; 4 µg/ml for western blot); anti-RNA Pol II CTD S5 rabbit polyclonal IgG antibody (Abcam, Cambridge, UK; ab52208; 2 µg/ml for western blot); anti-RPA194 rabbit polyclonal IgG antibody (Santa Cruz Biotechnology, Inc., Santa Cruz, CA, USA; sc-28714, clone H300; 1 µg/ml for western blot); anti-Son rabbit polyclonal IgG antibody (Abcam, Cambridge, UK; ab121759; 1 µg/ml for SIM and SCAN-R, 0.2 µg/ml for STED); anti-TFIID TBP rabbit polyclonal IgG antibody (Santa Cruz Biotechnology, Inc., Santa Cruz, CA, USA; sc-204; 2 µg/ml for SIM, 0.4 µg/ml for western blot); anti-TFIIEα rabbit polyclonal IgG antibody (Santa Cruz Biotechnology, Inc., Santa Cruz, CA, USA; sc28715; 0.4 µg/ml for western blot); anti-TFIIH p62 rabbit polyclonal IgG antibody (Santa Cruz Biotechnology, Inc., Santa Cruz, CA, USA; sc292; 0.4 µg/ml for western blot),

Secondary antibodies: donkey anti-human IgG (H+L) antibody conjugated with Cy5 (Jackson ImmunoResearch Laboratories, Inc., West Grove, PA, USA; 709-175-149; 1:50 for SIM); IRDye 680 donkey anti-mouse IgG (H+L) antibody (LI-COR Biosciences, Lincoln, NE, USA; 926-68072; 1:20000 for western blotting); donkey anti-rabbit IgG (H+L) antibody conjugated with Alexa Fluor 488 (Invitrogen, Thermo Fisher Scientific, Waltham, MA, USA; A21206; 5 µg/ml for SIM); IRDye 680 donkey anti-rabbit IgG (H+L) antibody (LI-COR Biosciences, Lincoln, NE, USA; 925-68073; 1:10000 for western blotting); IRDye 800 donkey anti-rabbit IgG (H+L) antibody (LI-COR Biosciences, Lincoln, NE, USA; 925-32213; 1:10000 and 1:20000 for western blotting); goat anti-mouse IgG (Fcγ fragment specific) antibody conjugated with DyLight 405 (Jackson ImmunoResearch Laboratories, Inc., West Grove, PA, USA; 115-475-071; 5 µg/ml for STED); goat anti-mouse IgG (Fcγ fragment specific) antibody conjugated with DyLight 488 (Jackson ImmunoResearch Laboratories, Inc., West Grove, PA, USA; 115-485-008; 1:100 for SIM and SCAN-R); goat anti-mouse IgG (Fcγ fragment specific) antibody coupled with 6 nm colloidal gold particles (Jackson ImmunoResearch Laboratories, Inc., West Grove, PA, USA; 115-195-071; 1:30 for TEM); goat anti-mouse IgM (µ-chain specific) antibody conjugated with Alexa Fluor 555 (Invitrogen, Thermo Fisher Scientific, Waltham, MA, USA; A21426; 5 µg/ml for SIM and SCAN-R); goat anti-mouse IgM (µ-chain specific) antibody conjugated with Alexa Fluor 568 (Invitrogen, Thermo Fisher Scientific, Waltham, MA, USA; A21043; 5 µg/ml for STED); goat anti-mouse IgM (µ-chain specific) antibody conjugated with Alexa Fluor 647 (Invitrogen, Thermo Fisher Scientific, Waltham, MA, USA; A21238; 5 µg/ml for SCAN-R); goat anti-mouse IgM (µ-chain specific) antibody coupled with 6 nm colloidal gold particles (Jackson ImmunoResearch Laboratories, Inc., West Grove, PA, USA; 115-195-075; 1:30 for TEM); goat anti-mouse IgM (µ-chain specific) antibody coupled with 12 nm colloidal gold particles (Jackson ImmunoResearch Laboratories, Inc., West Grove, PA, USA; 115-205-075; 1:30 for TEM); goat anti-rabbit IgG (H+L) antibody conjugated with Alexa Fluor 514 (Invitrogen, Thermo Fisher Scientific, Waltham, MA, USA; A31558; 5 µg/ml for STED); goat anti-

rabbit IgG (H+L) antibody conjugated with Alexa Fluor 647 (Invitrogen, Thermo Fisher Scientific, Waltham, MA, USA; A21245; 5 µg/ml for SIM and SCAN-R); goat anti-rabbit IgG (H+L) antibody coupled with 12 nm colloidal gold particles (Jackson ImmunoResearch Laboratories, Inc., West Grove, PA, USA; 111-205-144; 1:30 for TEM).

Acknowledgements. We are very thankful to Iva Jelínková, Lenka Jarolimová, Pavel Kříž, Ivana Nováková, and Jana Schrenková for their excellent technical work and to Irina Studenyak for her proofreading. We are grateful to Prof. Moise Bendayan for methodological tips. We thank Dr Enrique Castaño, Dr Matthias Merkenschlager, Dr Jeffrey Nickerson, Dr Iain Sawyer, Prof. David Spector, and Amy Strom for fruitful discussions. For financial support, we thank the Czech Science Foundation (GAP305/11/2232, GA16-03346S, and GA15-08738S); the Technology Agency of the Czech Republic (TE01020118); the Human Frontier Science Program (RGP0017/2013); the project 'BIOCEV – Biotechnology and Biomedicine Centre of the Academy of Sciences and Charles University' (CZ.1.05/1.1.00/02.0109) and the project 'Modernization and support of research activities of the national infrastructure for biological and medical imaging Czech-BioImaging' (CZ.02.1.01/0.0/0.0/16_013/0001775) from the European Regional Development Fund; the Czech Academy of Sciences (JSPS-18-18); the Institute of Molecular Genetics of the CAS (IMG; RVO:68378050); the Ministry of Education, Culture, Sports, Science and Technology of Japan (15H05902, 15K21738). The light microscopy data presented in this paper were produced at the Light Microscopy Core Facility, IMG of the CAS, Prague, Czech Republic, supported by the Ministry of Education, Youth and Sports of the Czech Republic (LM2015062); the Operational Program Prague – Competitiveness (CZ.2.16/3.1.00/21547) co-financed by the European Regional Development Fund; the National Programme of Sustainability I (LO1419) from the Ministry of Education, Youth and Sports of the Czech Republic. The electron microscopy data presented in this paper were produced at the Electron Microscopy Core Facility, IMG of the CAS, Prague, the Czech Republic, supported by the Ministry of Education, Youth and Sports of the Czech Republic (LM2015062 Czech-BioImaging).

The authors declare that they have no conflict of interest.

References

Almuzzaini, B., Sarshad, A. A., Farrants, A. K. and Percipalle, P. (2015). Nuclear myosin 1 contributes to a chromatin landscape compatible with RNA polymerase II transcription activation. *BMC Biol* **13**, 35.

Aronova, M. A. and Leapman, R. D. (2012). Development of Electron Energy Loss Spectroscopy in the Biological Sciences. *MRS Bull.* **37**, 53-62.

Balla, T. (2013). Phosphoinositides: tiny lipids with giant impact on cell regulation. *Physiol Rev* **93**, 1019-137.

Bendayan, M. (1981). Ultrastructural localization of nuclei acids by the use of enzyme-gold complexes. *J Histochem Cytochem* **29**, 531-41.

Bendayan, M. and Puvion, E. (1984). Ultrastructural localization of nucleic acids through several cytochemical techniques on osmium-fixed tissues: comparative evaluation of the different labelings. *J Histochem Cytochem* **32**, 1185-91.

Bickmore, W. A. and van Steensel, B. (2013). Genome Architecture: Domain Organization of Interphase Chromosomes. *Cell* **152**, 1270-1284.

Bolte, S. and Cordelieres, F. P. (2006). A guided tour into subcellular colocalization analysis in light microscopy. *Journal of Microscopy* **224**, 213-232.

Brangwynne, C. P., Mitchison, T. J. and Hyman, A. A. (2011). Active liquid-like behavior of nucleoli determines their size and shape in Xenopus laevis oocytes. *PNAS* **108**, 4334–4339.

Cavellan, E., Asp, P., Percipalle, P. and Farrants, A. K. (2006). The WSTF-SNF2h chromatin remodeling complex interacts with several nuclear proteins in transcription. *J Biol Chem* **281**, 16264-71.

Cheng, H. F., Jiang, M. J., Chen, C. L., Liu, S. M., Wong, L. P., Lomasney, J. W. and King, K. (1995). Cloning and identification of amino acid residues of human phospholipase C delta 1 essential for catalysis. *J Biol Chem* **270**, 5495-505.

Cheniclet, C. and Bendayan, M. (1990). Comparative pyrimidine- and purine-specific RNAse-gold labeling on pancreatic acinar cells and isolated hepatocytes. *J Histochem Cytochem* **38**, 551-62.

Cocco, L., Gilmour, R. S., Ognibene, A., Letcher, A. J., Manzoli, F. A. and Irvine, R. F. (1987). Synthesis of polyphosphoinositides in nuclei of Friend cells. Evidence for polyphosphoinositide metabolism inside the nucleus which changes with cell differentiation. *Biochem J* **248**, 765-70.

Dieck, C. B., Wood, A., Brglez, I., Rojas-Pierce, M. and Boss, W. F. (2012). Increasing phosphatidylinositol (4,5) bisphosphate biosynthesis affects plant nuclear lipids and nuclear functions. *Plant Physiol Biochem* **57**, 32-44.

Divecha, N., Banfic, H. and Irvine, R. F. (1991). The polyphosphoinositide cycle exists in the nuclei of Swiss 3T3 cells under the control of a receptor (for IGF-I) in the plasma membrane, and stimulation of the cycle increases nuclear diacylglycerol and apparently induces translocation of protein kinase C to the nucleus. *EMBO J* **10**, 3207-14.

Dunn, K. W., Kamocka, M. M. and McDonald, J. H. (2011). A practical guide to evaluating colocalization in biological microscopy. *Am J Physiol Cell Physiol* **300**, C723-C742.

Ferguson, K. M., Lemmon, M. A., Schlessinger, J. and Sigler, P. B. (1995). Structure of the high affinity complex of inositol trisphosphate with a phospholipase C pleckstrin homology domain. *Cell* **83**, 1037-46.

Feric, M., Vaidya, N., Harmon, T. S., Mitrea, D. M., Zhu, L., Richardson, T. M., Kriwacki, R. W., Pappu, R. V. and Brangwynne, C. P. (2016). Coexisting Liquid Phases Underlie Nucleolar Subcompartments. *Cell* **165**, 1686-1697.

Fujita, A., Cheng, J., Tauchi-Sato, K., Takenawa, T. and Fujimoto, T. (2009). A distinct pool of phosphatidylinositol 4,5-bisphosphate in caveolae revealed by a nanoscale labeling technique. *PNAS* **106**, 9256-9261.

Geeraerts, A., Hsiu-Fang, F., Zimmermann, P. and Engelborghs, Y. (2013). The characterization of the nuclear dynamics of syntenin-2, a PIP2 binding PDZ protein. *Cytometry A* **83**, 866-75.

Gonzales, M. L. and Anderson, R. A. (2006). Nuclear phosphoinositide kinases and inositol phospholipids. *J Cell Biochem* **97**, 252-60.

Gonzalez, I., Munita, R., Agirre, E., Dittmer, T. A., Gysling, K., Misteli, T. and Luco, R. F. (2015). A lncRNA regulates alternative splicing via establishment of a splicing-specific chromatin signature. *Nature Structural & Molecular Biology* **22**.

Harlan, J. E., Hajduk, P. J., Yoon, H. S. and Fesik, S. W. (1994). Pleckstrin homology domains bind to phosphatidylinositol-4,5-bisphosphate. *Nature* **371**, 168-70.

Hofmann, W. A., Vargas, G. M., Ramchandran, R., Stojiljkovic, L., Goodrich, J. A. and de Lanerolle, P. (2006). Nuclear myosin I is necessary for the formation of the first phosphodiester bond during transcription initiation by RNA polymerase II. *J Cell Biochem* **99**, 1001-9.

Hokanson, D. E., Laakso, J. M., Lin, T., Sept, D. and Ostap, E. M. (2006). Myo1c binds phosphoinositides through a putative pleckstrin homology domain. *Mol Biol Cell* **17**, 4856-65.

Hokanson, D. E. and Ostap, E. M. (2006). Myo1c binds tightly and specifically to phosphatidylinositol 4,5-bisphosphate and inositol 1,4,5-trisphosphate. *Proc Natl Acad Sci U S A* **103**, 3118-23.

Holcapek, M., Cífková, E., Cervená, B., Lísa, M., Vostálová, J. and Galuszka, J. (2015). Determination of nonpolar and polar lipid classes in human plasma,erythrocytes and plasma lipoprotein fractions usingultrahigh-performance liquid chromatography-mass spectrometry. *Journal of Chromatography A* **1377**, 85-91.

Iborra, F. J. (2007). Can visco-elastic phase separation, macromolecular crowding and colloidal physics explain nuclear organisation? *Theoretical Biology and Medical Modelling* **4**, 1-11.

Irvine, R. F. (2006). Nuclear inositide signalling -- expansion, structures and clarification. *Biochim Biophys Acta* **1761**, 505-8.

Janicki, S., Tsukamoto, T., Salghetti, S., Tansey, W., Sachidanandam, R., Prasanth, K., Ried, T., Shav-Tal, Y., Bertrand, E., Singer, R. et al. (2004). From Silencing to Gene Expression: Real-Time Analysis in Single Cells. *Cell* **116**, 683-698.

Jost, D., Carrivain, P., Cavalli, G. and Vaillant, C. (2014). Modeling epigenome folding: formation and dynamics of topologically associated chromatin domains. *Nucleic Acids Research* **42**, 9553-9561.

Lamond, A. I. and Spector, D. L. (2003). Nuclear speckles: a model for nuclear organelles. *Nat Rev Mol Cell Biol* **4**, 605-612.

Layerenza, J. P., Gonzalez, P., Garcia de Bravo, M. M., Polo, M. P., Sisti, M. S. and Ves-Losada, A. (2013). Nuclear lipid droplets: a novel nuclear domain. *Biochim Biophys Acta* **1831**, 327-40.

Lemmon, M. A., Ferguson, K. M., O'Brien, R., Sigler, P. B. and Schlessinger, J. (1995). Specific and high-affinity binding of inositol phosphates to an isolated pleckstrin homology domain. *Proc Natl Acad Sci U S A* **92**, 10472-6.

Lin, A., Hu, Q., Li, C., Xing, Z., Ma, G., Wang, C., Li, J., Ye, Y., Yao, J., Liang, K. et al. (2017). The LINK-A lncRNA interacts with PtdIns(3,4,5)P3 to hyperactivate AKT and confer resistance to AKT inhibitors. *Nature Cell Biology* **19**, 238-253.

Mao, Y. S., Sunwoo, H., Zhang, B. and Spector, D. L. (2011). Direct Visualization of the Co-transcriptional Assembly of a Nuclear Body by Noncoding RNAs. *Nat Cell Biol* **13**, 95–101.

Marmor, M. D. and Julius, M. (2001). Role for lipid rafts in regulating interleukin-2 receptor signaling. *Blood* **98**, 1489-97.

Mellman, D. L., Gonzales, M. L., Song, C., Barlow, C. A., Wang, P., Kendziorski, C. and Anderson, R. A. (2008). A PtdIns4,5P2-regulated nuclear poly(A) polymerase controls expression of select mRNAs. *Nature* **451**, 1013-7.

Micheli, M., Albi, E., Leray, C. and Magni, M. V. (1998). Nuclear sphingomyelin protects RNA from RNase action. *FEBS Letters* **431**, 443-447.

Mishkind, M., Vermeer, J. E., Darwish, E. and Munnik, T. (2009). Heat stress activates phospholipase D and triggers PIP accumulation at the plasma membrane and nucleus. *Plant J* **60**, 10-21.

Misteli, T. (2007). Beyond the Sequence: Cellular Organization of Genome Function. *Cell 128, 787–800* **128**, 787-800.

Mortier, E., Wuytens, G., Leenaerts, I., Hannes, F., Heung, M. Y., Degeest, G., David, G. and Zimmermann, P. (2005). Nuclear speckles and nucleoli targeting by PIP2-PDZ domain interactions. *EMBO J* **24**, 2556-65.

Ohsaki, Y., Kawai, T., Yoshikawa, Y., Cheng, J., Jokitalo, E. and Fujimoto, T. (2016). PML isoform II plays a critical role in nuclear lipid droplet formation. *J. Cell Biol.* **212**, 29-38.

Osborne, S. L., Thomas, C. L., Gschmeissner, S. and Schiavo, G. (2001). Nuclear PtdIns(4,5)P2 assembles in a mitotically regulated particle involved in pre-mRNA splicing. *J Cell Sci* **114**, 2501-11.

Pastorek, L., Sobol, M. and Hozák, P. (2016). Colocalization coefficients evaluating the distribution of molecular targets in microscopy methods based on pointed patterns. *Histochemistry and Cell Biology*, 1-16.

Payrastre, B., Nievers, M., Boonstra, J., Breton, M., Verkleij, A. J. and Van Bergen en Henegouwen, P. M. (1992). A differential location of phosphoinositide kinases, diacylglycerol kinase, and phospholipase C in the nuclear matrix. *J Biol Chem* **267**, 5078-84.

Percipalle, P., Fomproix, N., Cavellan, E., Voit, R., Reimer, G., Kruger, T., Thyberg, J., Scheer, U., Grummt, I. and Farrants, A. K. (2006). The chromatin remodelling complex WSTF-SNF2h interacts with nuclear myosin 1 and has a role in RNA polymerase I transcription. *EMBO Rep* **7**, 525-30.

Philimonenko, A. A., Janacek, J. and Hozak, P. (2000). Statistical evaluation of colocalization patterns in immunogold labeling experiments. *J Struct Biol* **132**, 201-10.

Philimonenko, V. V., Zhao, J., Iben, S., Dingova, H., Kysela, K., Kahle, M., Zentgraf, H., Hofmann, W. A., de Lanerolle, P., Hozak, P. et al. (2004). Nuclear actin and myosin I are required for RNA polymerase I transcription. *Nat Cell Biol* **6**, 1165-72.

Pombo, A., Jackson, D. A., Hollinshead, M., Wang, Z., Roeder, R. G. and Cook, P. R. (1999). Regional specialization in human nuclei: visualization of discrete sites of transcription by RNA polymerase III. *The EMBO Journal* **18**, 2241–2253.

Rando, O. J., Zhao, K., Janmey, P. and Crabtree, G. R. (2002). Phosphatidylinositol-dependent actin filament binding by the SWI/SNF-like BAF chromatin remodeling complex. *Proc Natl Acad Sci U S A* **99**, 2824-9.

Richter, K., Nessling, M. and Lichter, P. (2008). Macromolecular crowding and its potential impact on nuclear function. *Biochimica et Biophysica Acta* **1783**, 2100-2107.

Rossi, G., Magni, M. V. and Albi, E. (2007a). Signal transducer and activator of transcription 3 and sphingomyelin metabolism in intranuclear complex during cell proliferation. *Archives of Biochemistry and Biophysics* **464**, 138-143.

Rossi, G., Magni, M. V. and Albi, E. (2007b). Sphingomyelin-cholesterol and double stranded RNA relationship in the intranuclear complex. *Archives of Biochemistry and Biophysics* **459**, 27-32.

Saitoh, N., Spahr, C. S., Patterson, S. D., Bubulya, P., Neuwald, A. F. and Spector, D. L. (2004). Proteomic Analysis of Interchromatin Granule Clusters. *Molecular Biology of the Cell* **15**, 3876–3890.

Sarshad, A., Sadeghifar, F., Louvet, E., Mori, R., Bohm, S., Al-Muzzaini, B., Vintermist, A., Fomproix, N., Ostlund, A. K. and Percipalle, P. (2013). Nuclear myosin 1c facilitates the chromatin modifications required to activate rRNA gene transcription and cell cycle progression. *PLoS Genet* **9**, e1003397.

Scassellati, C., Albi, E., Cmarko, D., Tiberi, C., Cmarkova, J., Bouchet-Marquis, C., Verschure, P. J., Driel, R., Magni, M. V. and Fakan, S. (2010). Intranuclear sphingomyelin is associated with transcriptionally active chromatin and plays a role in nuclear integrity. *Biol Cell* **102**, 361-75.

Schaffer, B., Grogger, W. and Kothleitner, G. (2004). Automated spatial drift correction for EFTEM image series. *Ultramicroscopy* **102**, 27-36.

Schofer, C., Janacek, J., Weipoltshammer, K., Pourani, J. and Hozak, P. (2004). Mapping of cellular compartments based on ultrastructural immunogold labeling. *J Struct Biol* **147**, 128-35.

Sharma, A., Takata, H., Shibahara, K., Bubulya, A. and Bubulya, P. A. (2010). Son Is Essential for Nuclear Speckle Organization and Cell. *Molecular Biology of the Cell* **21**, 650-663.

Shen, X., Xiao, H., Ranallo, R., Wu, W. H. and Wu, C. (2003). Modulation of ATP-dependent chromatin-remodeling complexes by inositol polyphosphates. *Science* **299**, 112-4.

Shevtsov, S. P. and Dundr, M. (2011). Nucleation of nuclear bodies by RNA. *Nature Cell Biology* **13**.

Smith, J. J., Yakisich, J. S., Kapler, G. M., Cole, E. S. and Romero, D. P. (2004). A β-Tubulin Mutation Selectively Uncouples Nuclear Division and Cytokinesis in Tetrahymena thermophila. *EUKARYOTIC CELL* **3**, 1217-1226.

Sobol, M., Nebesarova, J. and Hozak, P. (2011). A method for preserving ultrastructural properties of mitotic cells for subsequent immunogold labeling using low-temperature embedding in LR White resin. *Histochem Cell Biol* **135**, 103-10.

Sobol, M., Philimonenko, V. V. and Hozak, P. (2010). Comparison of methods of high-pressure freezing and automated freeze-substitution of suspension cells combined with LR White embedding. *Histochem Cell Biol* **134**, 631-41.

Sobol, M., Yildirim, S., Philimonenko, V. V., Marasek, P., Castano, E. and Hozak, P. (2013). UBF complexes with phosphatidylinositol 4,5-bisphosphate in nucleolar organizer regions regardless of ongoing RNA polymerase I activity. *Nucleus* **4**, 478-86.

Stewart, S. A., Dykxhoorn, D. M., Palliser, D., Mizuno, H., Yu, E. Y., An, D. S., Sabatini, D. M., Chen, I. S. Y., Hahn, W. C., Sharp, P. A. et al. (2003). Lentivirus-delivered stable gene silencing by RNAi in primary cells. *RNA*, 493-501.

Stradalova, V., Gaplovska-Kysela, K. and Hozak, P. (2008). Ultrastructural and nuclear antigen preservation after high-pressure freezing/freeze-substitution and low-temperature LR White embedding of HeLa cells. *Histochem Cell Biol* **130**, 1047-52.

Strom, A. R., Emelyanov, A. V., Mir, M., Fyodorov, D. V., Darzacq, X. and Karpen, G. H. (2017). Phase separation drives heterochromatin domain formation. *Nature* **547**, 241-245.

Sugi, T., Oyama, T., Morikawa, K. and Jingami, H. (2008). Structural insights into the PIP2 recognition by syntenin-1 PDZ domain. *Biochem Biophys Res Commun* **366**, 373-8.

Tanaka, T., Iwawaki, D., Sakamoto, M., Takai, Y., Morishige, J., Murakami, K. and Satouchi, K. (2003). Mechanisms of accumulation of arachidonate in phosphatidylinositol in yellowtail. A comparative study of acylation systems of phospholipids in rat and the fish species Seriola quinqueradiata. *Eur J Biochem* **270**, 1466-73.

Thomas, C. L., Steel, J., Prestwichf, G. D. and Schiavo, G. (1999). Generation of phosphatidylinositol-specific antibodies and their characterization. *Biochemical Society Transactions* **27**, 648-652.

Toska, E., Campbell, H. A., Shandilya, J., Goodfellow, S. J., Shore, P., Medler, K. F. and Roberts, S. G. (2012). Repression of transcription by WT1-BASP1 requires the myristoylation of BASP1 and the PIP2-dependent recruitment of histone deacetylase. *Cell Rep* **2**, 462-9.

Trinkle-Mulcahy, L., Boulon, S., Lam, Y. W., Urcia, R., Boisvert, F. M., Vandermoere, F., Morrice, N. A., Swift, S., Rothbauer, U., Leonhardt, H. et al. (2008). Identifying specific protein interaction partners using quantitative mass spectrometry and bead proteomes. *J Cell Biol* **183**, 223-39.

Tripathi, V., Song, D. Y., Zong, X., Shevtsov, S. P., Hearn, S., Fu, X.-D., Dundr, M. and Prasanth, K. V. (2012). SRSF1 regulates the assembly of pre-mRNA processing factors in nuclear speckles. *Molecular Biology of the Cell* **23**, 3694-3706.

Ulicna, L., Kalendova, A., Kalasova, I., Vacik, T. and Hozák, P. (2018). PIP2 epigenetically represses rRNA genes transcription interacting with PHF8. *BBA - Molecular and Cell Biology of Lipids* **1863**, 266-275.

Uzbekov, R. and Roingeard, P. (2013). Nuclear lipid droplets identified by electron microscopy of serial sections. *BMC Res Notes.* **6**, 1-4.

Vann, L. R., Wooding, F. B., Irvine, R. F. and Divecha, N. (1997). Metabolism and possible compartmentalization of inositol lipids in isolated rat-liver nuclei. *Biochem J* **327 (Pt 2)**, 569-76.

Venit, T., Dzijak, R., Kalendová, A., Kahle, M., Rohožková, J., Schmid, t. V., Rülicke, T., Rathkolb, B., Hans, V., Bohla, A. et al. (2013). Mouse nuclear myosin I knock-out shows interchangeability and redundancy of myosin isoforms in the cell nucleus. *PLoS One* **in press**.

Wang, J., Arbuzova, A., Hangyas-Mihalyne, G. and McLaughlin, S. (2001). The effector domain of myristoylated alanine-rich C kinase substrate binds strongly to phosphatidylinositol 4,5-bisphosphate. *J Biol Chem* **276**, 5012-9.

Watt, S. A., Kular, G., Fleming, I. N., Downes, C. P. and Lucocq, J. M. (2002). Subcellular localization of phosphatidylinositol 4,5-bisphosphate using the pleckstrin homology domain of phospholipase C delta1. *Biochem J* **363**, 657-66.

Wright, R. (2000). Transmission electron microscopy of yeast. *Microsc Res Tech* **51**, 496-510.

Xu, M. and Cook, P. R. (2008). Similar active genes cluster in specialized transcription factories. *J. Cell Biol.* **181**, 615-623.

Ye, J., Zhao, J., Hoffmann-Rohrer, U. and Grummt, I. (2008). Nuclear myosin I acts in concert with polymeric actin to drive RNA polymerase I transcription. *Genes Dev* **22**, 322-30.

Yildirim, S., Castano, E., Sobol, M., Philimonenko, V. V., Dzijak, R., Venit, T. and Hozak, P. (2013). Involvement of phosphatidylinositol 4,5-bisphosphate in RNA polymerase I transcription. *J Cell Sci* **126**, 2730-9.

Yoo, S. H., Huh, Y. H., Huh, S. K., Chu, S. Y., Kim, K. D. and Hur, Y. S. (2014). Localization and projected role of phosphatidylinositol 4-kinases IIalpha and IIbeta in inositol 1,4,5-trisphosphate-sensitive nucleoplasmic Ca(2)(+) store vesicles. *Nucleus* **5**, 341-51.

Yu, H., Fukami, K., Watanabe, Y., Ozaki, C. and Takenawa, T. (1998). Phosphatidylinositol 4,5-bisphosphate reverses the inhibition of RNA transcription caused by histone H1. *Eur J Biochem* **251**, 281-7.

Zhao, K., Wang, W., Rando, O. J., Xue, Y., Swiderek, K., Kuo, A. and Crabtree, G. R. (1998). Rapid and phosphoinositol-dependent binding of the SWI/SNF-like BAF complex to chromatin after T lymphocyte receptor signaling. *Cell* **95**, 625-36.

Zimmermann, P., Meerschaert, K., Reekmans, G., Leenaerts, I., Small, J. V., Vandekerckhove, J., David, G. and Gettemans, J. (2002). PIP(2)-PDZ domain binding controls the association of syntenin with the plasma membrane. *Mol Cell* **9**, 1215-25.

Figures

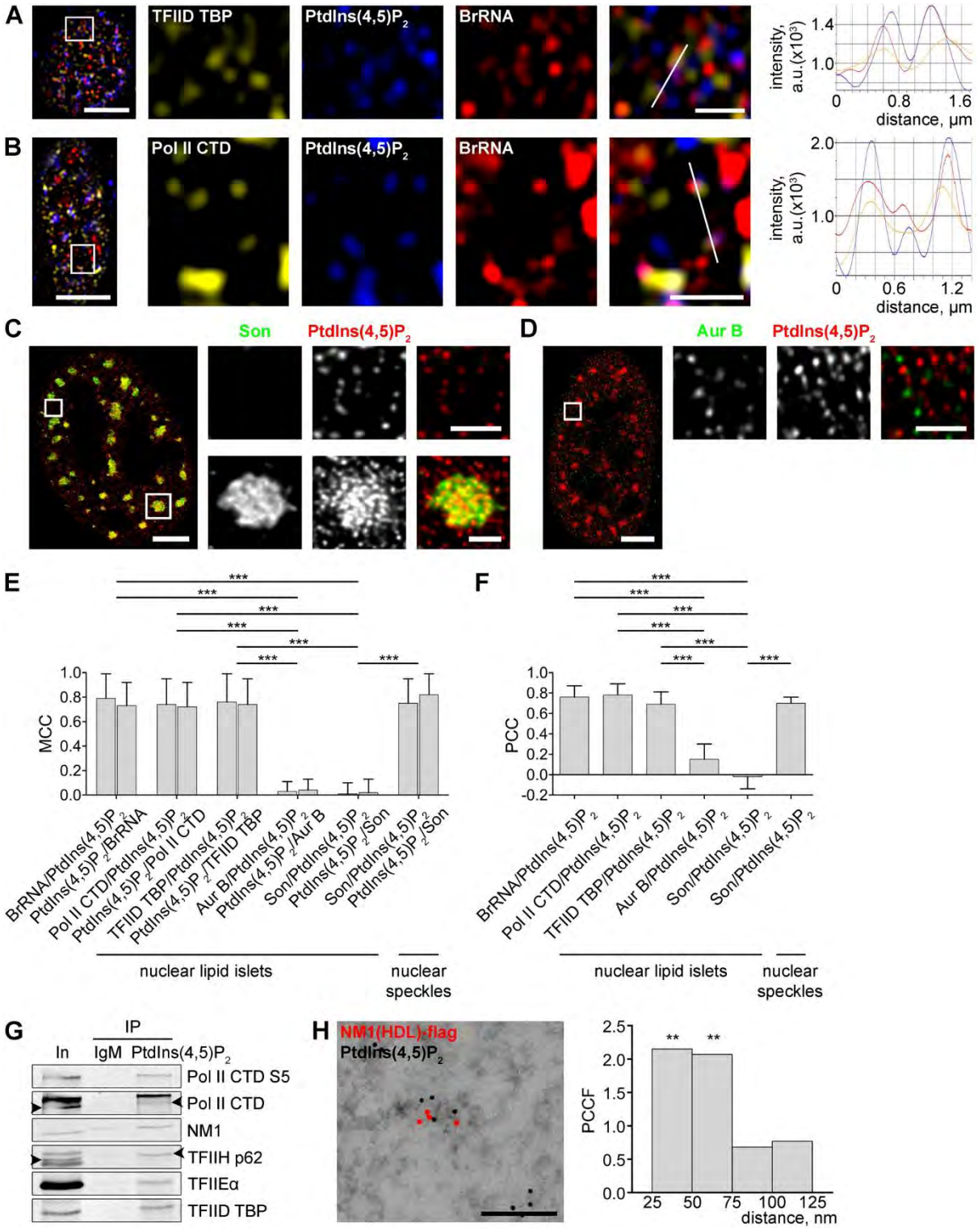

Figure 1. Nucleoplasmic PtdIns(4,5)P_2 appears in small foci which colocalise with nascent RNA and proteins involved in Pol II transcription. (A, B) Immunofluorescent labelling followed

by SIM demonstrates that nucleoplasmic PtdIns(4,5)P_2 forms small foci and colocalises with both nascent RNA transcripts (BrRNA) and the TATA-box binding protein (TBP) of the Pol II transcription factor TFIID (TFIID TBP) as well as the C-terminal domain of the Pol II largest subunit (Pol II CTD). This colocalisation is documented as well by intensity profiles. General view: bar is 5 μm; magnified view corresponds to the area outlined by the white rectangle: bar is 1 μm. (C, D) Immunofluorescent labelling followed by STED shows that neither Son nor Aurora B kinase (Aur B) colocalises with nucleoplasmic PtdIns(4,5)P_2 foci. In contrast, Son colocalises with PtdIns(4,5)P_2 in nuclear speckles (C, magnified view, the bottom row). General view: bar is 5 μm; magnified views correspond to the areas outlined by the white rectangles: bar is 1 μm. (E, F) The analysis of the colocalisation between PtdIns(4,5)P_2, nascent BrRNA, Pol II CTD, TFIID TBP, Son, and Aurora B kinase was done separately for each nucleoplasmic PtdIns(4,5)P_2 focus. Likewise the colocalisation between PtdIns(4,5)P_2 and Son was analysed for each nuclear speckle. (E) Manders' colocalisation coefficients (MCCs), presented as the mean ± standard deviation (s.d.), exhibit colocalisation between PtdIns(4,5)P_2 and nascent BrRNA (n = 74), PtdIns(4,5)P_2 and Pol II CTD (n = 49), and between PtdIns(4,5)P_2 and TFIID TBP (n = 25). MCC shows no colocalisation between PtdIns(4,5)P_2 and either Son (n = 515) or Aurora B kinase (n = 300) in the foci and indicates that PtdIns(4,5)P_2 and Son colocalise in nuclear speckles (n = 81); $p \leq 0.001$. (F) Pearson's correlation coefficients (PCCs), showed as the mean ± s.d., exhibit colocalisation between PtdIns(4,5)P_2 and BrRNA (n = 74), Pol II CTD (n = 49), and TFIID TBP (n = 25), respectively. PCC demonstrates no significant colocalisation between PtdIns(4,5)P_2 and either Son (n = 515) or Aurora B kinase (n = 300) in the foci and shows that PtdIns(4,5)P_2 and Son are colocalised in nuclear speckles (n = 81); $p \leq 0.001$. (G) Nuclear extracts were subjected to immunoprecipitation with anti-PtdIns(4,5)P_2 antibody and L-protein magnetic beads. Western blots show the specific association of PtdIns(4,5)P_2 with Pol II CTD, including its phosphorylated form at serine 5 – Pol II CTD S5, NM1, the p62 core subunit of TFIIH (TFIIH p62), the large subunit of TFIIE (TFIIEα), and TFIID TBP. The control mouse monoclonal IgM antibody used for immunoprecipitation shows no signal (IP/IgM). For better recognition and distinguishing of the specific bands for Pol II CTD and TFIIH p62, which are close to the neighbouring bands for Pol II CTD S5 and TFIIEα, respectively, we put the arrowheads in the lines of input (In) and anti-PtdIns(4,5)P_2 antibody immunoprecipitates (IP/PtdIns(4,5)P_2). (H) The cells transiently transfected with a truncated form of NM1 fused to flag-tag (NM1(HDL)-flag) were processed for TEM and double-labelled with anti-flag and anti-PtdIns(4,5)P_2 antibodies. TEM showed more accurately that these PtdIns(4,5)P_2 foci are structures of 40–100 nm in diameter and revealed the presence of NM1 at the periphery of these structures. Based on their shape and size, we refer to them as nuclear lipid islets (NLIs). Bar is 200 nm. The graph shows that PtdIns(4,5)P_2 molecules and NM1 significantly colocalise at the distance of 25–75 nm (n = 21, PCCF > 1, $p \leq 0.01$).

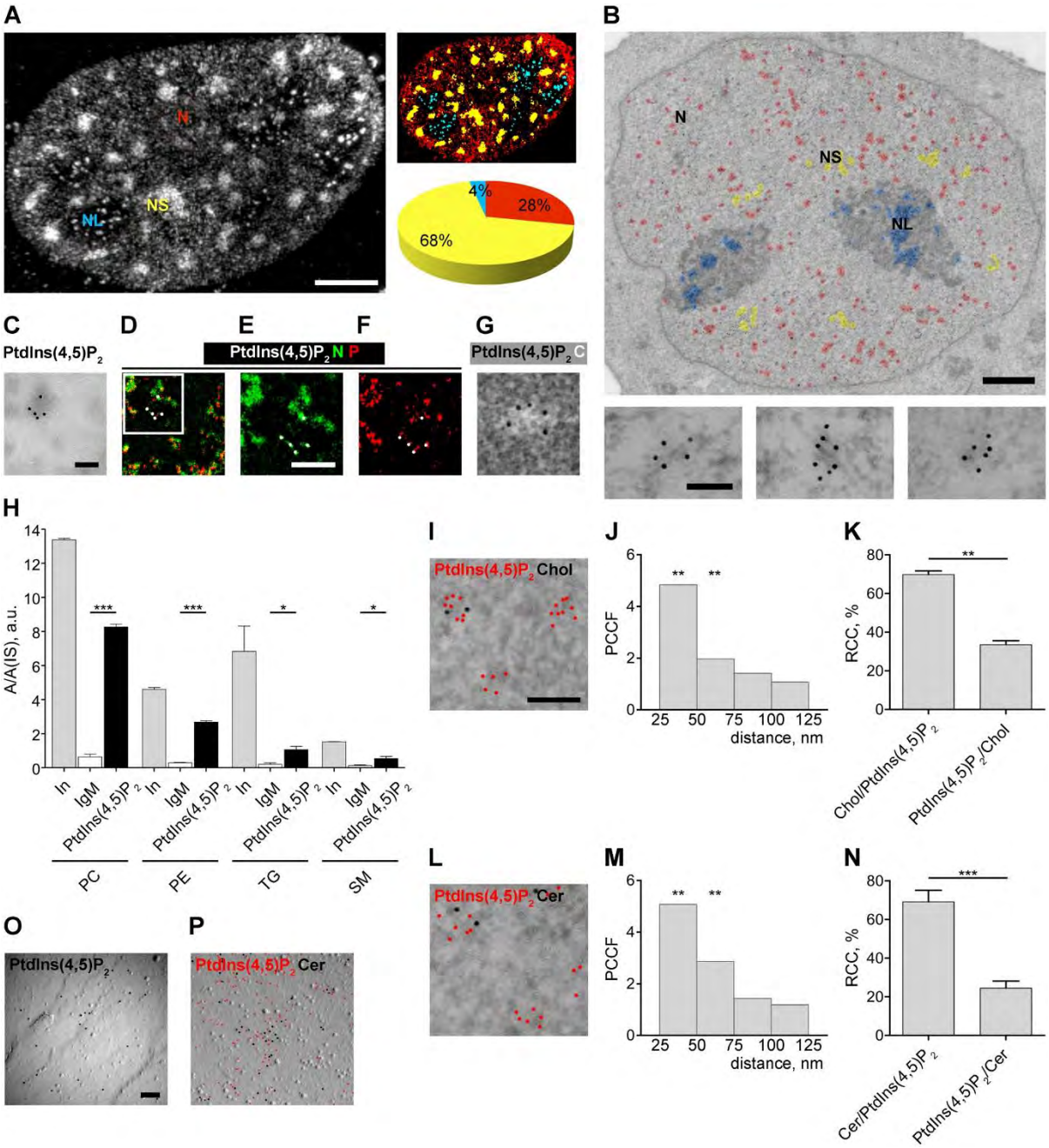

Figure 2. The morphology, composition and distribution of NLIs. (A) PtdIns(4,5)P_2 was visualised with anti-PtdIns(4,5)P_2 antibody and the z-stack was acquired using SIM. Nuclear PtdIns(4,5)P_2 labelling was reconstructed in 3D and shown here as 2D maximum intensity projection image: N – nucleus, NS – nuclear speckles, NL – nucleolus; bar is 1 µm. The distribution of PtdIns(4,5)P_2 in nuclear speckles, nucleoli, and the nucleoplasm was calculated in 3D, and the PtdIns(4,5)P_2 present in the nuclear speckles, nucleoli, and the nucleoplasm was colour-coded using the NIS-Elements and MATLAB software. The colour-coded original 2D image and diagram are shown on the right: the PtdIns(4,5)P_2 in nuclear speckles is shown in yellow, the PtdIns(4,5)P_2 in the nucleoplasm is in red, and the nucleolar PtdIns(4,5)P_2 is in blue. (B) A TEM image of nuclear

PtdIns(4,5)P_2 labelling on the surface of an ultrathin section. The abbreviations and colour-coding are the same as in (A). NLIs of 40–100 nm are shown in magnified view below. Mapping was done using the commercially available software Ellipse (ViDiTo, Kosice, Slovakia) with the additionally installed software Gold plugins (Philimonenko et al., 2000; Schofer et al., 2004). General view: bar is 1 µm, magnified views: bar is 100 nm. (C) Ultrathin sections were first labelled with anti-PtdIns(4,5)P_2 antibody, followed by the secondary antibody conjugated with gold nanoparticles, and further subjected to elemental mapping by EELS; bar is 100 nm for (C) and (D). (D) The elemental mapping of the presence of nitrogen (N, in green) and phosphorus (P, in red) in NLIs. PtdIns(4,5)P_2 is marked by the nanoparticles covered co-centrically with white dots for (D), (E), and (F). (E, F) Magnified view of (D) shows NLI surrounded by nitrogen- (E) and phosphorus-containing structures (F); bar is 100 nm for (E), (F), and (G). The inner part of NLI appears to be devoid of them both. (G) Carbon (C, in white) mapping shows the inner space of NLI enriched with carbon-rich compounds. (H) A HeLa nuclear extract was subjected to immunoprecipitation with anti-PtdIns(4,5)P_2 antibody, after which the lipidic component of the immunoprecipitate was analysed using hydrophilic interaction liquid chromatography – ultrahigh-performance liquid chromatography/electrospray ionisation – mass spectrometry (HILIC-UHPLC/ESI-MS). The graph shows the amount of lipids quantified as the ratio of the peak areas corresponding to lipid classes in a base–peak chromatogram (*m/z* 570–900) (A) to the peak area of the internal standard (A(IS)) in arbitrary units (a.u.). Data from two independent experiments are presented as the mean ± s.d. Major lipidic constituents specifically associated with PtdIns(4,5)P_2 (PtdIns(4,5)P_2), as compared to the control mouse monoclonal IgM antibody used for immunoprecipitation (IgM), are phosphatidylcholines (PC), phosphatidylethanolamines (PE), triacylglycerols (TG), and sphingomyelins (SM) ($p \leq 0.001$, $p \leq 0.001$, $p \leq 0.05$, and $p \leq 0.05$, respectively). PC, PE, TG, and SM were also identified in the input nuclear extract (In). (I) Ultrathin sections were simultaneously labelled with anti-PtdIns(4,5)P_2 antibody and anti-cholesterol antibody, followed by secondary antibodies conjugated with 6 nm and 12 nm gold nanoparticles, respectively. TEM reveals that cholesterol molecules (Chol) are located on the surface of NLIs; bar is 100 nm for (I) and (L). (J) The graph shows that PtdIns(4,5)P_2 molecules and cholesterol are significantly colocalised at the distances of 25–75 nm (PCCF > 1.5, $p \leq 0.01$, n = 20). (K) The graph displays the relative colocalisation (RCC) of cholesterol with PtdIns(4,5)P_2 molecules (Chol/PtdIns(4,5)P_2) and *vice versa* (PtdIns(4,5)P_2/Chol) as the mean ± s.d. ($p \leq 0.01$). (L) Ultrathin sections were first labelled on one side with anti-PtdIns(4,5)P_2 antibody, followed by the secondary antibody conjugated with 6 nm gold nanoparticles. Then the sections were labelled on the other side with an anti-ceramide antibody, followed by the secondary antibody conjugated with 12 nm gold nanoparticles. TEM detects ceramide molecules (Cer) on the surface of NLIs. (M) The graph shows that PtdIns(4,5)P_2 molecules and ceramide are significantly colocalised at the distances of 25–75 nm (PCCF > 1.5, $p \leq 0.01$, n = 41). (N) The graph displays the relative colocalisation (RCC) of ceramide with PtdIns(4,5)P_2 molecules (Cer/PtdIns(4,5)P_2) and *vice versa* (PtdIns(4,5)P_2/Cer) as the mean ± s.d. ($p \leq 0.001$). (O,

P) Replicas of HeLa cells prepared using high-pressure freezing and freeze-fracturing were labelled with either anti-PtdIns(4,5)P_2 antibody (O) or GST-tagged PLC PH domain, followed by anti-GST antibody together with anti-ceramide antibody (P). Both labellings exhibit a pattern similar to (B), (I), and (L), confirming that NLIs are native nucleoplasmic structures. Bar is 100 nm for (O) and (P).

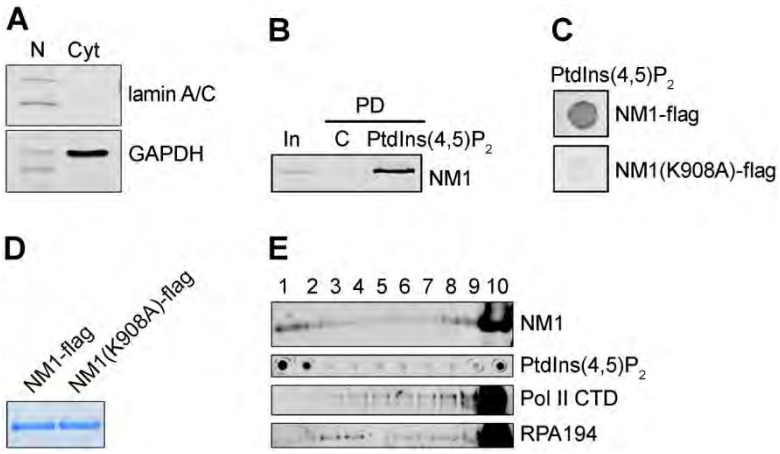

Figure 3. NM1 associates with NLIs and is anchored in the nucleoplasm by PtdIns(4,5)P_2. (A) Nuclear extract was checked for a purity by immunoblotting with anti-lamin A/C antibody. N – nuclear extract, Cyt – cytoplasmic extract. (B) NM1 was pulled-down with PtdIns(4,5)P_2-coupled agarose beads from the nuclear extract and detected by immunoblotting. Control beads show no signal. In – input nuclear extract, PD – nuclear extract pulled down with either PtdIns(4,5)P_2-coupled agarose beads (PtdIns(4,5)P_2) or control beads (C). (C) Direct binding of NM1 to PtdIns(4,5)P_2 was confirmed by an incubation of recombinant wild-type NM1-flag and its PtdIns(4,5)P_2-binding mutant NM1(K908A)-flag with PtdIns(4,5)P_2 spotted on a nitrocellulose membrane. The recombinant NM1-flag and NM1(K908A)-flag were immunodetected by an anti-flag antibody. (D) To ensure the equal loading of NM1 and NM1(K908A) in the experiment shown in (C), their amount was assessed by SDS-PAGE. (E) The nuclei extracted by Brij98 were subjected to flotation on a sucrose density gradient. The nuclear extract was placed to the bottom of the gradient. After centrifugation, fractions were subjected to SDS-PAGE, transferred to a nitrocellulose membrane and immunodetected for the presence of NM1, Pol II, and Pol I. To detect PtdIns(4,5)P_2, fractions were spotted on a nitrocellulose membrane and labelled with anti-PtdIns(4,5)P_2 antibody. Both NM1 and PtdIns(4,5)P_2 are present in the light fraction 1, containing detergent-insoluble lipoprotein complexes, and also in the heavy fraction 10, composed of soluble complexes. In contrast, Pol II CTD and RPA194 (the largest subunit of Pol I) are mainly revealed in the detergent-soluble heavy fraction (number 10).

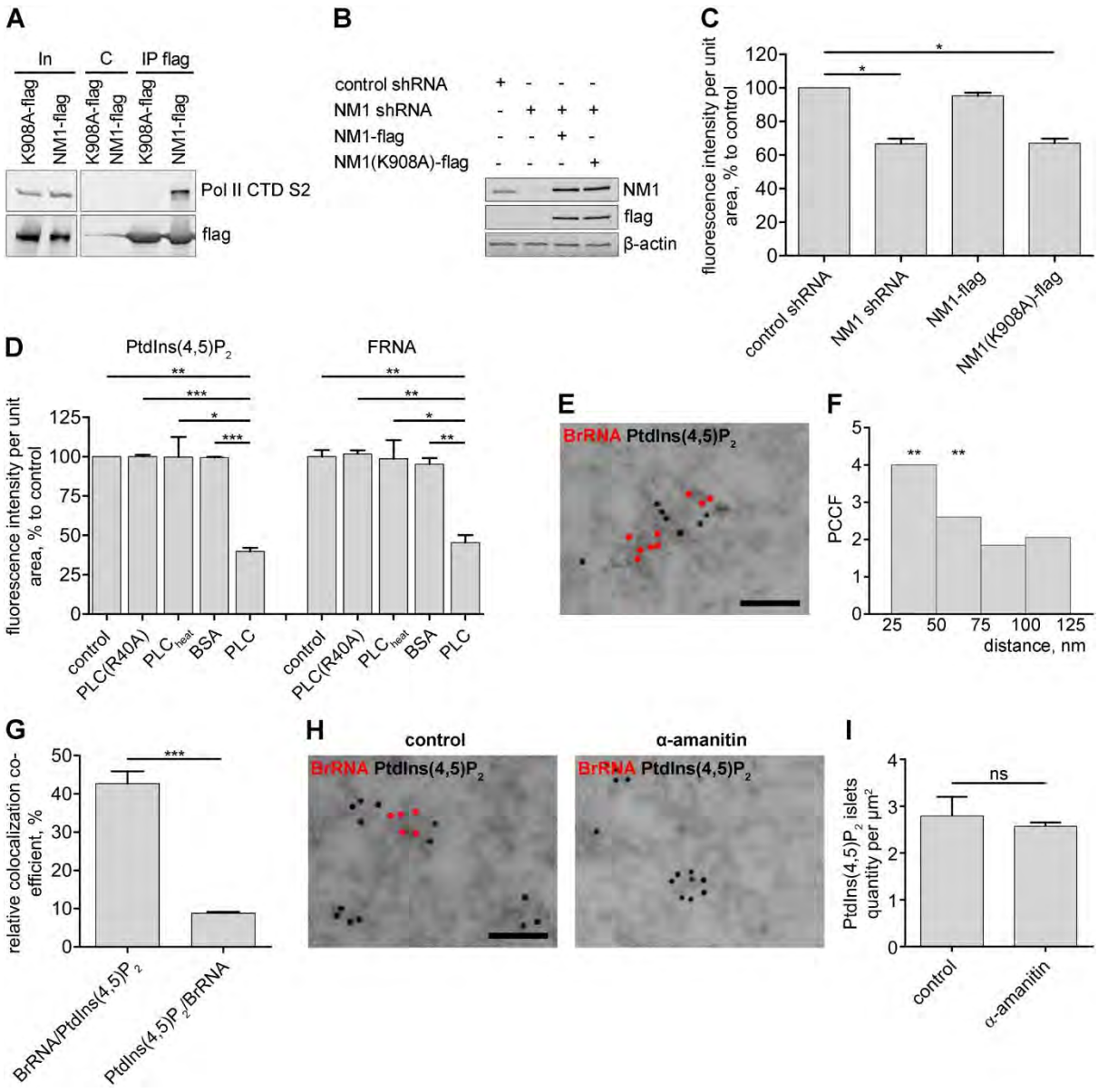

Figure 4. PtdIns(4,5)P_2-NM1 interaction and the integrity of NLIs are important for Pol II-dependent transcription. (A) Cells stably expressing NM1-flag or NM1(K908A)-flag were lysed and subjected to co-immunoprecipitation by anti-flag antibody. Immunoprecipitates were analysed by anti-Pol II CTD S2 and anti-flag antibodies. Only NM1, which is able to bind PtdIns(4,5)P_2, associates with Pol II as well. (B) Using shRNA-mediated knock-down, we generated a stable cell line with decreased expression of NM1. On top of that, we further introduced the shRNA-resistant NM1-flag or NM1(K908A)-flag. As a control, a cell line expressing non-targeting shRNA was used. (C) We monitored the Pol II transcription level in the cell lines outlined in (B) by pulse-labelling of nascent transcripts with FU. We immunolabelled FU with anti-BrdU antibody and quantified the intensity of the signal by indirect high-throughput immunofluorescent microscopy. The data from two independent experiments are presented as fluorescence intensity per unit area in percent relative to the control value (mean ± s.d.); control shRNA n = 1677, NM1 shRNA n = 2219, NM1 shRNA/NM1-flag

n = 1930, NM1 shRNA/NM1(K908A)-flag n = 1322. The depletion of NM1 by shRNA-mediated knock-down resulted in a decreased level of Pol II transcription ($p \leq 0.05$). The overexpression of NM1 rescued Pol II transcription close to its original level, while the overexpression of PtdIns(4,5)P_2-binding mutant NM1(K908A) had no effect. (D) For PtdIns(4,5)P_2 hydrolysis, cells were permeabilised and incubated with PLC. As a control, the cells were incubated with either PLC(R40A), which is unable to bind PtdIns(4,5)P_2, or heat-inactivated PLC, or BSA, or buffer only. After 30 min, FU was added to the cells. FU as well as PtdIns(4,5)P_2 were visualised with the appropriate antibodies and the intensity was quantified using indirect high-throughput immunofluorescent microscopy. Data from two independent experiments are presented as the intensity of fluorescence per unit area of NLIs in percent to a control value (the mean ± s.d.); control n = 915, PLC(R40A) n = 830, PLC_{heat} n = 920, BSA n = 398, PLC n = 854. A decrease of the PtdIns(4,5)P_2 level by hydrolysis ($p \leq 0.01$) resulted in the reduction of the Pol II transcription level in the NLI area ($p \leq 0.01$). PLC(R40A), inactivated PLC, or BSA had no effect either on the level of PtdIns(4,5)P_2 or on the level of Pol II transcription. (E) Cells were incubated with BrUTP as a precursor for RNA synthesis. Then the cells were processed for TEM and double-labelled with anti-BrdU and anti-PtdIns(4,5)P_2 antibodies. We clearly show here that PtdIns(4,5)P_2 molecules form the islets colocalised at their periphery with nascent RNA transcripts. Bar is 100 nm. (F) The graph represents the colocalisation between PtdIns(4,5)P_2 molecules and BrRNA at the distances of 25–75 nm (n = 59, PCCF > 2, $p \leq 0.01$). (G) The graph shows the relative colocalisation of BrRNA and PtdIns(4,5)P_2 molecules (BrRNA/PtdIns(4,5)P_2) and *vice versa* (PtdIns(4,5)P_2/BrRNA) as the mean ± s.d. (n = 59, $p \leq 0.001$). (H) TEM clearly demonstrates that upon inhibition of Pol II transcription with α-amanitin, the appearance of NLIs was indistinguishable from the control. Bar is 100 nm. (I) The graph shows that the quantity of NLIs per μm^2 in the nuclei of cells treated with α-amanitin was not significantly changed as compared to the control cells ($p \geq 0.05$). The data are presented as the mean ± s.d., control n = 59, α-amanitin n = 213.

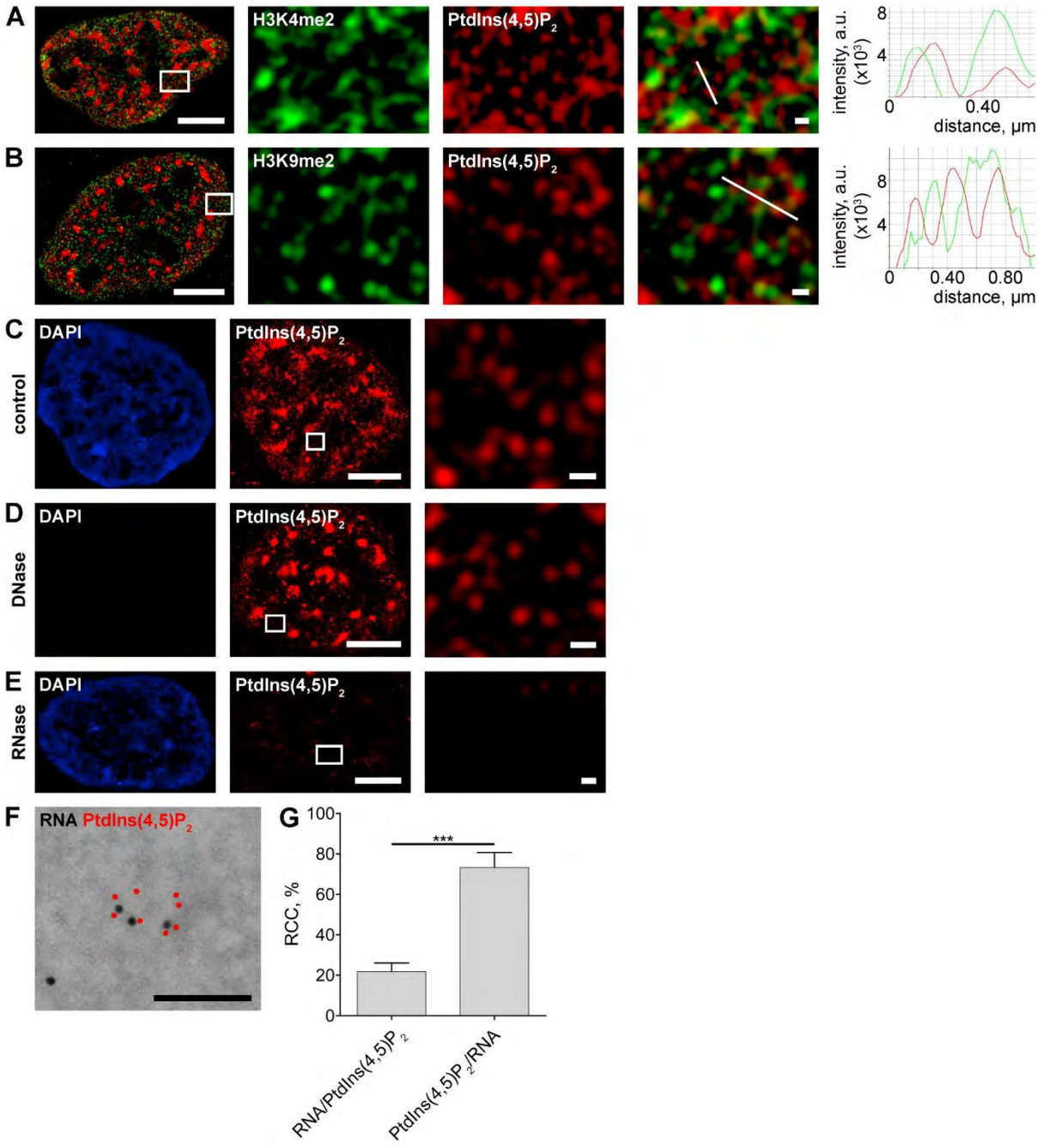

Figure 5. NLIs are chromatin-independent, while RNA is an essential component for their integrity. (A, B) Immunofluorescent labelling followed by SIM reveals that NLIs partially overlap with either histone H3K4me2 enriched in transcriptionally active genes (A) or histone H3K9me2, which is a heterochromatin marker (B), as confirmed by fluorescence intensity profiles. General view: bar is 5 µm; magnified view corresponds to the area outlined by the white rectangle: bar is 200 nm. (C, D) Immunofluorescent labelling followed by SIM demonstrates that the treatment of cells with 250 U/ml DNase for 30 min (D) has no significant effect on the arrangement of NLIs as compared to the control (C). (E) Cells treated with 1 mg/ml RNase for 30 min display almost complete disappearance of NLI labelling. General view: bar is 5 µm; magnified view corresponds to the area

outlined by the white rectangle: bar is 200 nm. (F) Ultrathin sections were first labelled with anti-PtdIns(4,5)P_2 antibody followed by secondary antibody conjugated with 6 nm gold nanoparticles. Then the sections were labelled with RNase conjugated with 10 nm gold nanoparticles. TEM demonstrates that RNA molecules are located on the surface of NLIs; bar is 100 nm. (G) The graph shows the relative colocalisation of RNA with PtdIns(4,5)P_2 molecules (RNA/PtdIns(4,5)P_2) and *vice versa* (PtdIns(4,5)P_2/RNA) as the mean ± s.d. ($n = 37$, $p \leq 0.001$).

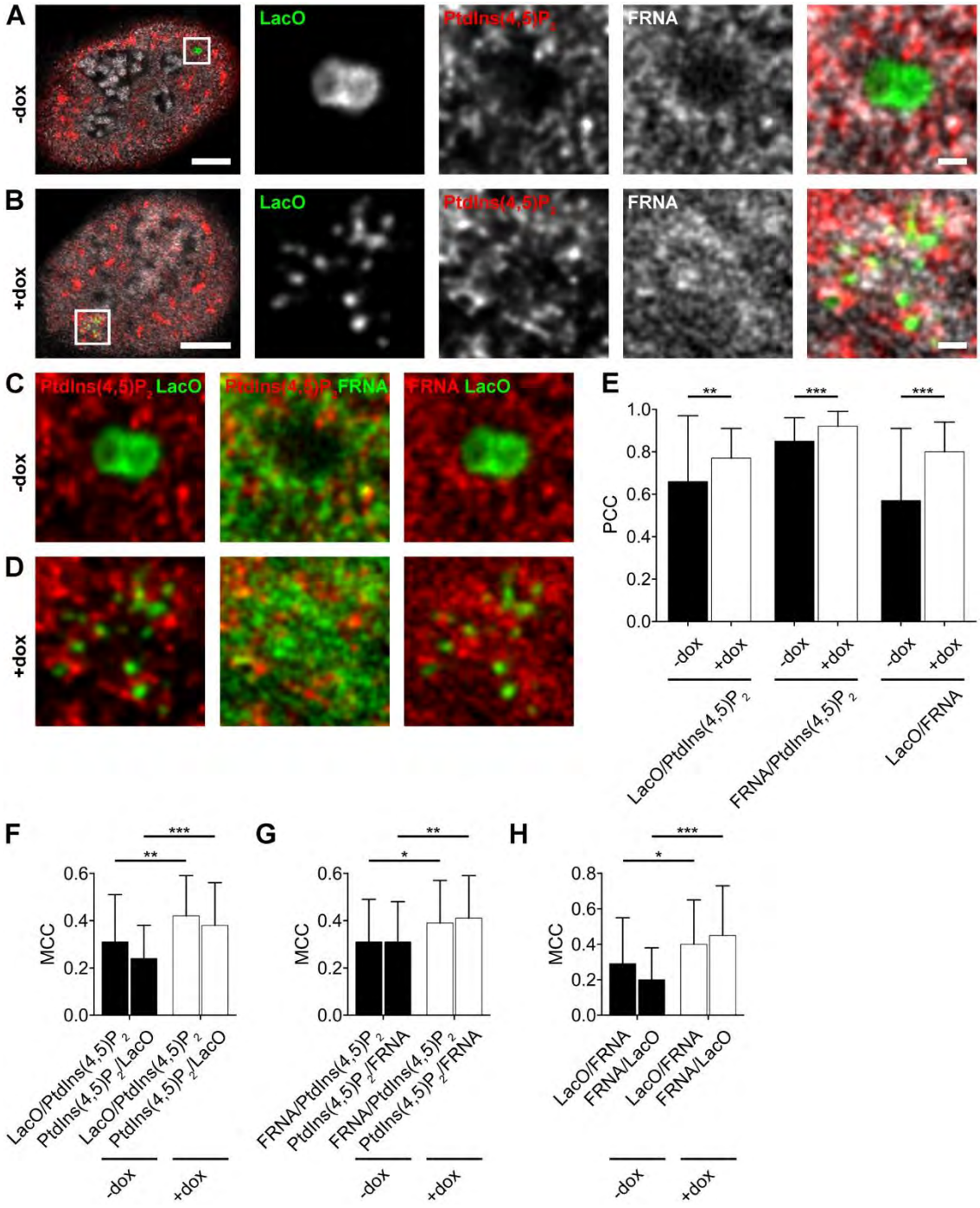

Figure 6. DNA can dynamically re-associate with NLIs; transcriptionally active foci are preferentially located on the surface of NLIs. (A, B) U2OS 2-6-3 cells, stably expressing p3216PECMS2β plasmid, were co-transfected with the tetracycline-controlled transactivator and the EYFP-lac repressor, pulse-labelled with FU, fixed and immunolabelled. (A) STED showed that the condensed transgene locus (LacO), marked by the EYFP-lac repressor, colocalises with neither NLIs nor nascent transcripts (FRNA). (B) The induction of transcription after addition of dox to the medium resulted in the colocalisation of the decondensed locus with NLIs and nascent transcripts. General views: bar is 5 μm; magnified views correspond to the areas outlined by the white rectangles:

bar is 500 nm. (C, D) The colocalisation between PtdIns(4,5)P_2, LacO, and FRNA was analysed for each NLI taken separately. (E) PCC, shown as the mean ± s.d., exhibits colocalisation for the pairs: LacO and PtdIns(4,5)P_2, FRNA and PtdIns(4,5)P_2, LacO and FRNA before (-dox) and after (+dox) transcription induction; $p \leq 0.01$, $p \leq 0.001$, and $p \leq 0.001$, respectively (-dox n = 58, +dox n = 49). (F, G, H) MCC, presented as the mean ± s.d., displays the extent of colocalisation between LacO and PtdIns(4,5)P_2 (F), FRNA and PtdIns(4,5)P_2 (G), LacO and FRNA (H) before (-dox) and after (+dox) induction of transcription. The effect of transcription induction is clearly visible by the increased extent of colocalisation between transgene foci and NLIs ($p \leq 0.01$ and $p \leq 0.001$, F), nascent transcripts and NLIs ($p \leq 0.05$ and $p \leq 0.01$, G), transgene foci and nascent transcripts ($p \leq 0.05$ and $p \leq 0.001$, H).

Supplementary figures

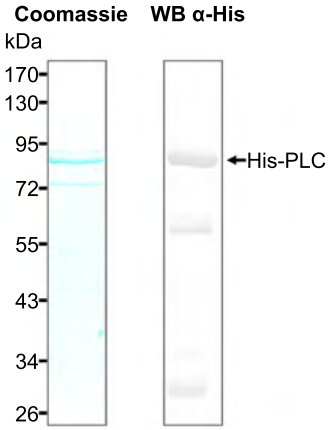

Supplementary Figure 1. The purity of recombinant PLC. Expressed and purified His-tagged PLC was detected in the eluted fraction using Coomassie staining and western blotting (WB) with anti-His antibody.

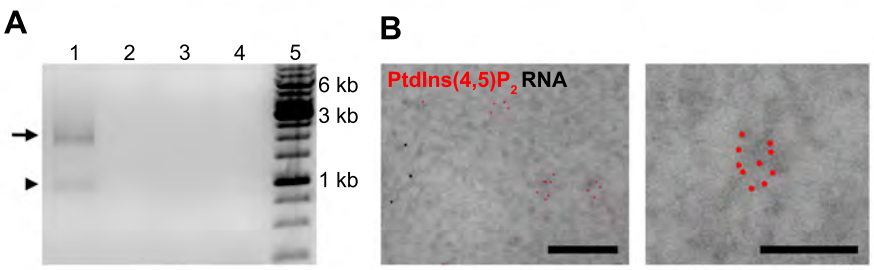

Supplementary Figure 2. The activity of RNase-gold complex and its labelling specificity. (A) The enzymatic activity of RNase after conjugation with gold nanoparticles was assessed using *in vitro* incubation with RNA followed by agarose gel electrophoresis; lane 1 – input RNA, lane 2 – RNA treated with RNase before conjugation, lane 3 – RNA treated with unbound RNase after conjugation, lane 4 – RNA treated with the RNase-gold complex, lane 5 – marker. The cleaved 28 S (arrow) and 18S RNA (arrowhead) proves the activity of the complex. (B) The labelling specificity of the RNase-gold complex was tested by TEM. Prior to the labelling, the RNase-gold complex was presaturated *in vitro* with RNA. This mixture was then used for the labelling of the sections. Apparent depletion of labelling proves the specificity of labelling by the RNase-gold complex. The general view: the bar is 200 nm; the magnified view: the bar is 100 nm.

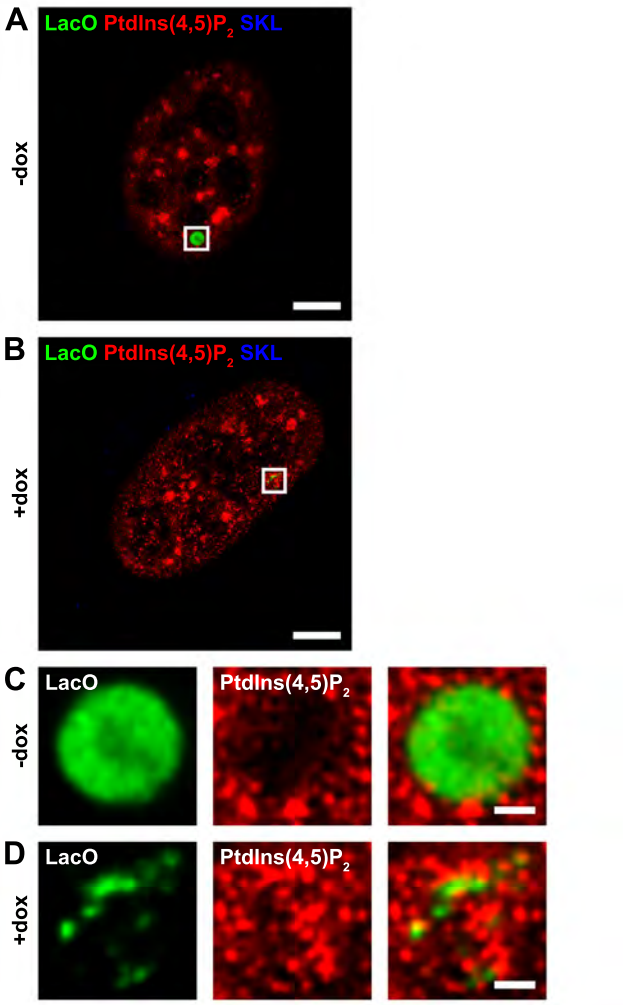

Supplementary Figure 3. The induction of the transcription of the transgene locus. (A) U2OS 2-6-3 cells stably expressing p3216PECMS2β plasmid were co-transfected with the tetracycline-controlled transactivator and the EYFP-lac repressor, fixed, immunolabelled with the anti-PtdIns(4,5)P_2 antibody and visualized by STED. (B) The addition of dox to the medium induced transcription of the transgene locus, which was confirmed by the appearance of CFP-SKL in cytoplasmic peroxisomes. The general view: the bar is 5 µm. (C, D) The induction of transcription was reinforced by noticeable changes in the arrangement of transgene foci. The magnified views correspond to the areas outlined by the white rectangles in (A) and (B), respectively; the bar is 500 nm.